



HAL
open science

Interpretable ensemble machine learning for the prediction of the expansion of cementitious materials under external sulfate attack

Benoit Hilloulin, Abdelhamid Hafidi, Sonia Boudache, Ahmed Loukili

► **To cite this version:**

Benoit Hilloulin, Abdelhamid Hafidi, Sonia Boudache, Ahmed Loukili. Interpretable ensemble machine learning for the prediction of the expansion of cementitious materials under external sulfate attack. Journal of Building Engineering, 2023, pp.107951. 10.1016/j.jobbe.2023.107951 . hal-04255480

HAL Id: hal-04255480

<https://nantes-universite.hal.science/hal-04255480v1>

Submitted on 24 Oct 2023

HAL is a multi-disciplinary open access archive for the deposit and dissemination of scientific research documents, whether they are published or not. The documents may come from teaching and research institutions in France or abroad, or from public or private research centers.

L'archive ouverte pluridisciplinaire **HAL**, est destinée au dépôt et à la diffusion de documents scientifiques de niveau recherche, publiés ou non, émanant des établissements d'enseignement et de recherche français ou étrangers, des laboratoires publics ou privés.

Journal Pre-proof

Interpretable ensemble machine learning for the prediction of the expansion of cementitious materials under external sulfate attack

Benoît Hilloulin, Abdelhamid Hafidi, Sonia Boudache, Ahmed Loukili



PII: S2352-7102(23)02131-9

DOI: <https://doi.org/10.1016/j.jobe.2023.107951>

Reference: JOBE 107951

To appear in: *Journal of Building Engineering*

Received Date: 21 August 2023

Revised Date: 7 October 2023

Accepted Date: 14 October 2023

Please cite this article as: Benoît Hilloulin, A. Hafidi, S. Boudache, A. Loukili, Interpretable ensemble machine learning for the prediction of the expansion of cementitious materials under external sulfate attack, *Journal of Building Engineering* (2023), doi: <https://doi.org/10.1016/j.jobe.2023.107951>.

This is a PDF file of an article that has undergone enhancements after acceptance, such as the addition of a cover page and metadata, and formatting for readability, but it is not yet the definitive version of record. This version will undergo additional copyediting, typesetting and review before it is published in its final form, but we are providing this version to give early visibility of the article. Please note that, during the production process, errors may be discovered which could affect the content, and all legal disclaimers that apply to the journal pertain.

© 2023 Published by Elsevier Ltd.

Interpretable Ensemble Machine Learning for the prediction of the expansion of cementitious materials under external sulfate attack

Benoît Hilloulin*, Abdelhamid Hafidi, Sonia Boudache, Ahmed Loukili

Nantes Université, Ecole Centrale Nantes, CNRS, GeM, UMR 6183, F-44000 Nantes, France – e-mail: benoit.hilloulin@ec-nantes.fr

*Corresponding author: Benoit.Hilloulin@ec-nantes.fr

Abstract

External sulfate attack (ESA) is a key degradation mechanisms of cementitious materials. Although the advantages of low- C_3A cement and supplementary cementitious materials (SCM) have been confirmed, there remains a need for a better understanding of the phenomenon and guidance on accelerated testing due to the numerous parameters affecting this degradation. This study introduces a machine learning framework for predicting the expansion of cementitious materials incorporating SCM because of ESA. A comprehensive database is constructed, and four optimized machine learning models are compared. Among them, extreme Gradient Boosting (XGBoost) showed the best performance with a R^2 accuracy of 0.933 and 0.788 on the training and the test set resp. Additionally, SHapley Additive exPlanations (SHAP) enabled the identification of the most influential inputs and their relative influence. It has been found that clinker composition, mix proportion, sample geometry, and sulfate solution characteristics play an important role, with their relative contribution being 34%, 36%, 3% and 27% resp. Furthermore, a thorough analysis of the model predictions on some expansive and non-expansive mortar and concrete samples demonstrated its reliability. Finally, the model was shown to be able to accurately predict the time required to reach a given expansion.

Keywords: Concrete; Sulfate attack; Expansion, Machine Learning; SHAP.

1. Introduction

Among all the degradations that can happen to cementitious materials, the external sulfate attack is one of the most studied and documented. The attack mechanism can be summarized as follows: sulfates in solution progress into the cement matrix by diffusion and react with ions in the

30 pore solution to form expansive products. The most common expansive product is the
31 aluminosulfate phase ettringite [1]. According to the crystal pressure theory [2], secondary
32 ettringite forming from a supersaturated pore solution into the cement matrix nanoporosity will
33 lead to expansion and, after that, cracking [3,4].

34 Many lab tests have been performed to highlight the parameters influencing ESA. Those
35 parameters can be related to the sulfate solution, the conditions of exposure, or the cementitious
36 material properties. First, the type of cation and the sulfate concentration of the sulfate solution
37 directly impact the products formed during the attack. The magnesium reacts with hydrates from
38 the cement paste to form brucite and M-S-H that replace C-S-H during magnesium sulfate attack
39 [5]. Gypsum will form over ettringite when the sulfate solution has a sulfate concentration of over
40 30 g/L [6,7]). A high sulfate concentration accelerates the diffusion of sulfates. The supersaturation
41 regarding ettringite is reached faster: the higher the sulfate concentration, the shorter the response
42 time [8]. Secondly, exposure conditions such as pH and temperature also affect the kinetic of the
43 attack. A controlled pH of 7 spurs the $\text{Ca}(\text{OH})_2$ leaching [9] and subsequently provides Ca^{2+} to the
44 pore solution that can react with sulfate to form expansive products [10]. While high temperatures
45 induce a shortening in response time, temperatures below 5 °C lead to the formation of calcium
46 sulfate carbonate phase, e.g., thaumasite, as a product of ESA [11].

47 While sulfate solution and exposure conditions greatly influence the ESA mechanism, most
48 of the chemical elements reacting with sulfates are brought by the cement matrix. The clinker C_3A
49 content is considered the most important aluminates source. Thus CEM I cement with low C_3A
50 content are considered sulfate-resistant cements (SR0, SR3, SR5) [12]. SCM such as slag, fly ash
51 or pozzolans consume portlandite by pozzolanic reactions and form C-A-S-H besides the C-S-H
52 formed by C_3S and C_2S hydration, lessening the gypsum formation and ettringite recrystallization
53 [13]. Recently, the positive effect of calcined clay has been reported [14,15]. The fine porosity of
54 C-A-S-H slows the sulfate diffusion through the cementitious matrix and has a positive effect on
55 the resistance to ESA. Last, diffusion being controlled by porosity, the water/cement ratio greatly
56 affects the sulfate resistance of a sample [16]. However, the behavior of the ternary or quaternary
57 cement blends with high substitution ratios remains an open question.

58 The collected information helps set up more efficient and representative lab tests. One of the
59 most debated points is the duration of the test because of the number of parameters influencing the
60 time to reach a given expansion. As stated before, the formation of expansive products will depend

61 on the sulfate concentration in the pore solution; the sulfate diffusion is thus the limiting step. Tests
62 may require several months before giving significant results. Thus, to address this issue, some lab
63 tests are designed to accelerate the degradation process. While they may be effective, it is difficult
64 to say if they are accurate to the ESA mechanism [17]. Moreover, the relative importance of the
65 various parameters involved in ESA is still debated. For example, mortar and concrete mix
66 compositions and samples' geometrical features play a decisive role in the volumetric expansion
67 measured in laboratory tests, influencing the final classification of types of cement regarding their
68 sulfate resistance.

69 In recent years, Machine Learning has been increasingly employed for predicting and
70 analyzing cementitious materials' properties. Deep Learning techniques and Convolutional Neural
71 networks help assess concrete properties at various scales: from crack and defect detection [18–
72 20] to concrete microscopic image analysis [21–23] or mechanical properties [24]. Gaussian
73 processes, Bayesian techniques, and exploration-exploitation techniques close to reinforcement
74 learning have been successfully employed to infer mechanical characteristics from
75 microindentation and nanoindentation [25] or quantitatively estimate uncertainties concerning
76 concrete properties such as susceptibility to sulfate degradation [26]. However, these techniques
77 are relatively limited in terms of interpretability. For this reason, supervised learning models have
78 been further developed as they can be accompanied by mature interpretability tools in order to gain
79 insights about the most influencing parameters governing a phenomenon. Numerous research
80 works have been published to predict concrete compressive strength [27–30], fresh properties [31],
81 creep [32,33], shrinkage [34–36], chloride [37], carbonation resistance [38], frost resistance [39].
82 Advances such as features analysis and dubbed SHapley Additives exPlanations (SHAP) [40]
83 introduced novel ways to explore feature impact, and it has been shown that machine learning can
84 provide similar or better predictions than analytical models [36]. However, to the authors'
85 knowledge, no study has been reported to predict the expansion of mortar and concrete samples
86 due to external sulfate attack using machine learning, even though such models would help identify
87 the major influencing parameters, the role of SCM, and likely help provide guidelines relative to
88 the laboratory tests definition towards a quick and representative expansion assessment.

89 This study provides insight into the potential of machine learning models based on
90 conventional or ensemble techniques to predict the expansion of cementitious materials, eventually
91 incorporating supplementary cementitious materials due to the external sulfate attack. A database

92 has been specifically built based on the available literature. The theory and procedures associated
93 with the models are briefly presented in the manuscript. Then, the results of the models are
94 discussed, and the best model candidate is further examined using SHapley Additive exPlanation
95 (SHAP) theory to understand the most influential features and derive partial difference plots.
96 Finally, a comparison is made between the experimental and predicted time to reach specific
97 expansions.

98 **2. Database description and initial processing**

99 **2.1 Database construction**

100 Observations of linear expansions of samples completely immersed in sulfate solutions, also
101 called length variations, were selected from different sources in the literature [8,13,14,17,41–64].
102 These studies reported expansions of various mortar and concrete specimens with sulfate-resistant
103 and non-sulfate-resistant cement from standard to high-strength mixes. Only mixes based on CEM
104 I cements, eventually with SCM (fly ash, slag, pozzolan, limestone, silica fume and calcined clay,
105 abbreviated with MK in Table 1), were selected because of the lack of information about some
106 standardized blended cement (classified as CEM II to CEM V according to Eurocodes). In total,
107 336 mortar and concrete expansion curves were obtained and used to interpolate expansion values
108 at increasing ages relative to the square root of time due to the diffusive nature of the process, e.g.,
109 $1\sqrt{d}$, $2\sqrt{d}$, $3\sqrt{d}$, ..., until the end of each corresponding measurement. Then, after the interpolation
110 and the filtering steps, 5294 expansion data points were generated. Only positive expansions
111 smaller than 0.4% were considered in order to limit the influence of external phenomena on the
112 results, such as leaching or extensive cracking. Some curves were not included because of
113 excessive or very rapid unexplained expansions. No further cleaning or filtering was applied.

114 Four types of inputs parameters were considered: clinker composition (C_3S , C_2S , C_3A and
115 C_4AF), mix proportion and characteristics (cement mass, aggregate-to-cement ratio, water-to-
116 binder ratio and SCMs proportions, 28-day compressive strength reflecting porosity which is rarely
117 reported), sample geometry (shape and surface-to-perimeter ratio), and sulfate solution and
118 environment characteristics (cation type, concentration, pH, and temperature). Categorical values
119 such as cation type and mold properties were encoded to be used as inputs in the model. We
120 attributed the value 1 to Na, the value 0 to Mg, and, concerning the mold shape, we attributed the
121 value 0 for prismatic specimens and 1 for cylindrical specimens.

2.2 Imputation of missing values

2.2.1 Compressive strength inference using XGBoost

Since porosity and strength-related properties might have an influence on expansion during the external sulfate attack process and considering that strength is reported more often than porosity [63], a dedicated XGBoost model has been used to input missing 28-day compressive strength data, amounting to 44% of the database (148 formulations), based on the cement composition and the mix formulation as described in the previous section. The choice has been made to demonstrate the suitability of the present database without the need for an external database. The model has been trained using 75% of the 188 experimental compressive strengths available in the original database and tested on the remaining 25%. Between 20 and 80 MPa, the 28-day cubic compressive strength of the test samples was estimated with an R^2 value of 0.83, which is better than the classic mean inference or regression methods. All missing strength values were thus inferred using the dedicated XGBoost model.

2.2.2 Other missing values

Two different methods were used to infer other missing values [17-19]. First, the univariate imputation consists of filling in the missing values by statistical characteristics of the existing data (median, most frequent, mean). This simple approach is used for the missing oxides in the cement composition. The second method, relying on the physical aspects, is used for pH. Due to leaching phenomena, the missing values of uncontrolled pH are filled by 10. Last, missing C_3S , C_2S , C_3A , and C_4AF values were calculated using Bogue's equation based on oxides compositions.

2.3. Final database description

After inferring all missing values, the final database containing 5294 expansion values relative to 21 parameters was obtained. A description of the database is given in Table 1, and the cumulated distribution functions associated with most of the inputs are given in Fig. 1. Mean and median values have been reported, as well as minimum and maximum values. The database covers a wide range of cement compositions, mortar and concrete formulations with various W/B ratios, SCM types, and sulfate solution compositions and environmental conditions. No particular data imbalance can be observed. However, temperature values were almost all equal to 20 or 23°C and nanosilica content equal to 0%, their effects cannot thus be analyzed in-depth.

151 Correlations between the input variables were calculated before the machine learning
 152 algorithms' application in order to avoid excessive correlations between variables. The correlation
 153 matrix is given in Fig. 2. As expected, some formulation parameters (water-binder ratio, water-
 154 binder ratio, aggregate-cement ratio, and cement content) were particularly correlated. Apart from
 155 these correlations concerning formulations, no other significant correlation was observed.

156

157 **Table 1.** Description of the database used in this study

	mean	std	min	25%	50%	75%	max
C ₃ S (%)	57.7	5.9	34.0	54.95	56.66	61.0	73.5
C ₂ S (%)	14.9	6.0	2.29	12.0	14.57	18.1	39.0
C ₃ A (%)	8.0	2.6	0.9	5.8	7.6	10.1	11.9
C ₄ AF (%)	9.4	2.7	0.0	7.8	9.7	10.98	19.7
Cement (kg/m ³)	355.4	129.5	55.0	269	375	469	553
A/C	4.36	1.9	1.64	3.0	3.9	5.2	15.4
W/B	0.5	0.08	0.33	0.48	0.5	0.55	0.77
Fly Ash (%mb)	3.6	25.8	0.0	0.0	0.0	0.0	50.0
Slag (%mb)	14.3	23.6	0.0	0.0	0.0	20.0	85.0
Pozzolan (%mb)	0.25	3.5	0.0	0.0	0.0	0.0	50.0
Limestone (%mb)	2.9	8.6	0.0	0.0	0.0	0.0	50.0
MK (%mb)	2.37	7.0	0.0	0.0	0.0	0.0	34.0
Silica Fume (%mb)	0.29	1.6	0.0	0.0	0.0	0.0	13.0
Nanosilica (%mb)	0.30	1.2	0.0	0.0	0.0	0.0	8.0
Cation	0.5	0.5	0.0	1.0	1.0	1.0	1.0
Concentration %	5.7	5.1	0.3	3.0	5.0	5.0	20.0
pH	9.0	1.8	3.0	7.5	10.0	10.0	12.3
Temperature (°C)	19.5	4.7	1.0	20.0	20.0	20.	35.0
Mold properties	0.04	0.2	0.0	0.0	0.0	0.0	1.0
Surface/perimeter (cm)	1.0	0.6	0.25	0.625	0.625	1.25	2.5
fc28 (MPa)	49.4	13.4	20.6	41.5	47.9	54	100

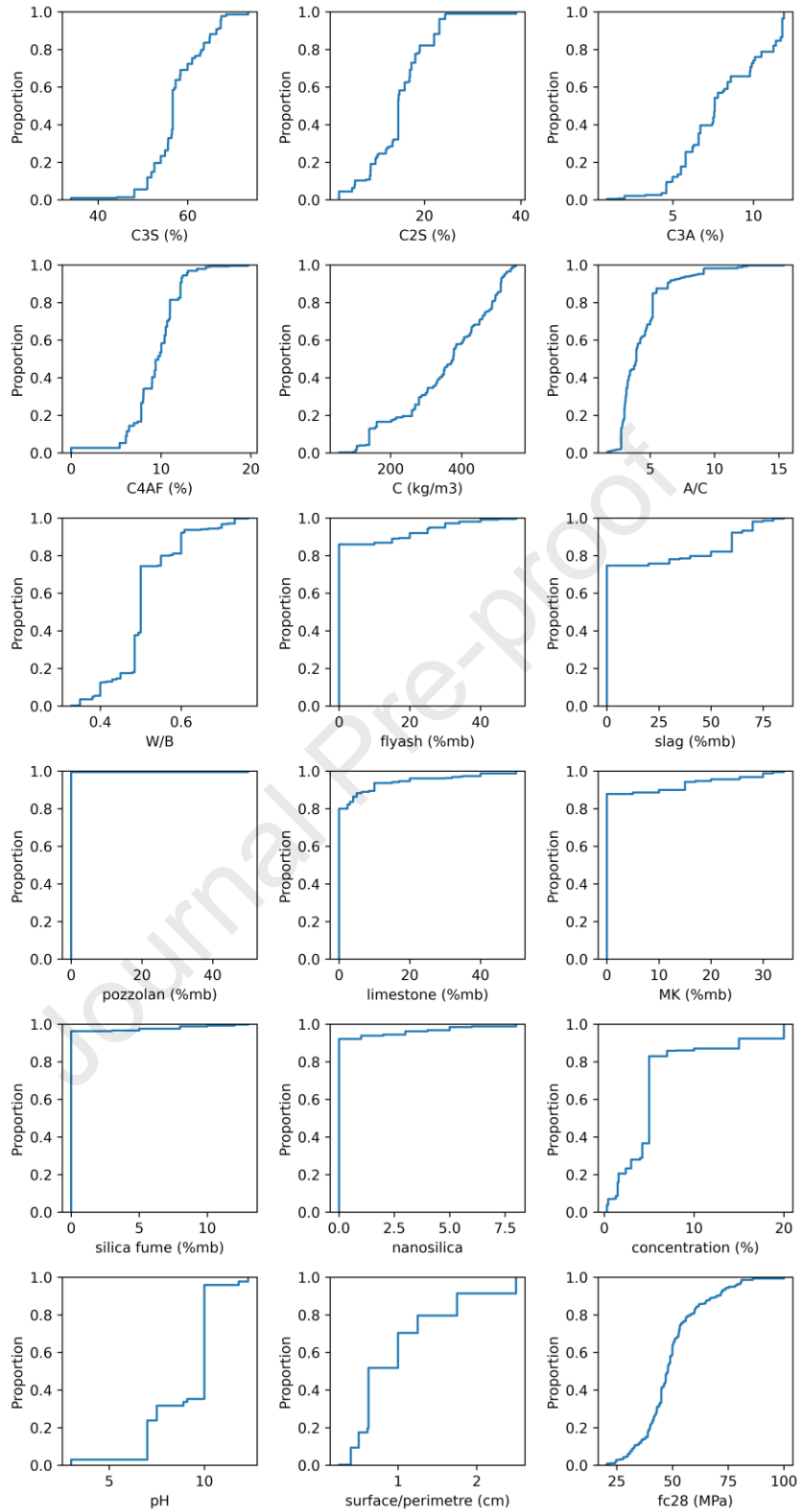
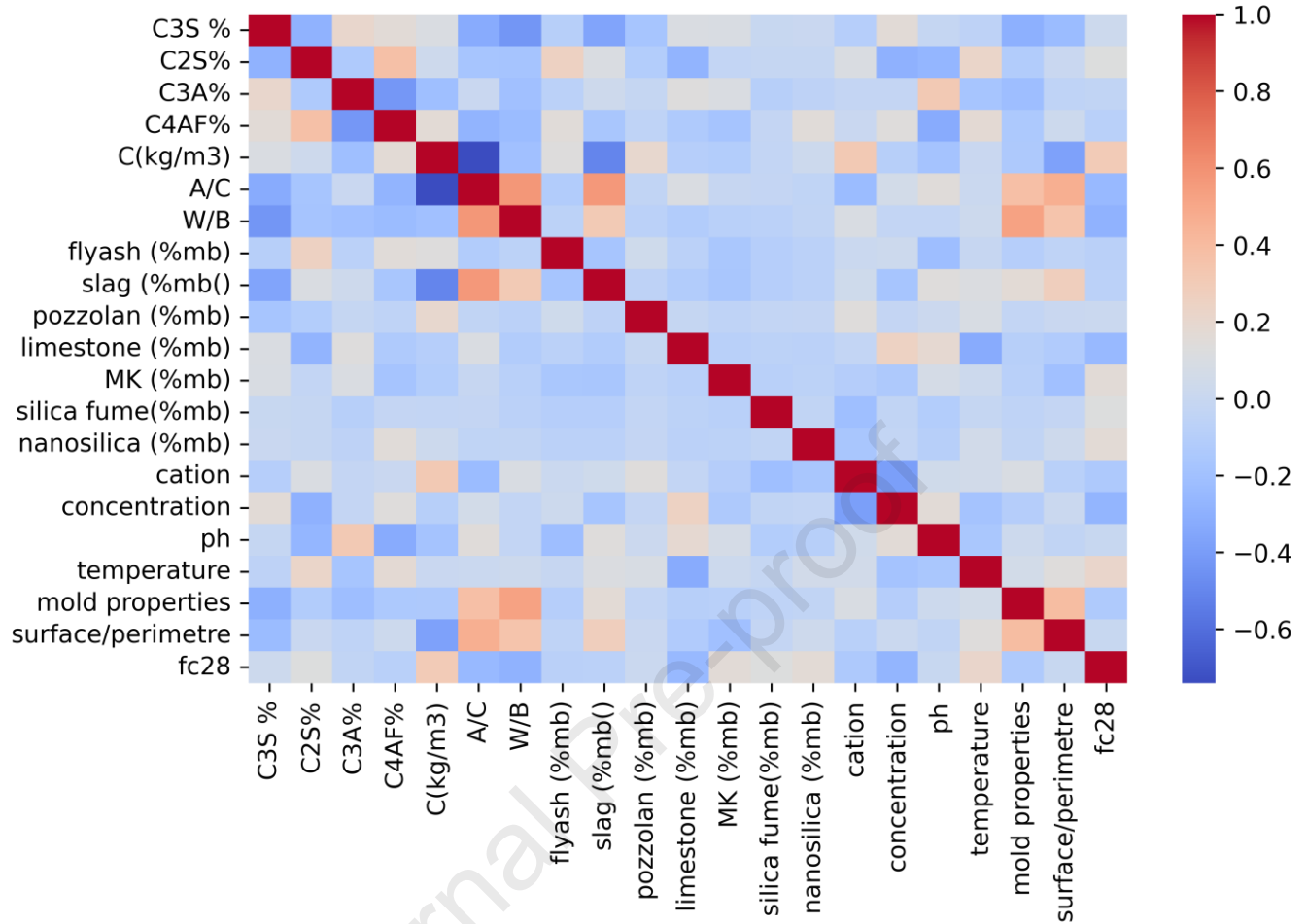


Fig 1. Experimental cumulative distribution functions of the inputs



160
161 **Fig. 2.** Correlation matrix of the input variables

162 **3. Methods**

163 **3.1. Machine learning models**

164 **3.1.1 Linear regression**

165 Regression analysis was first provided by Francis Galton in the second half of the 19th
 166 century. Regression analysis is a statistical approach that uses the relation between quantitative
 167 variables, so that a simple linear curve can predict a result or response variable [65]. Regression
 168 models have only linear parameters; therefore, the predicted variables are linear. The linear curve
 169 is constructed to have a lesser error between the variables and the curve. Linear regression (LR) is
 170 used as a benchmark model in this study to highlight the benefits of using ensemble models.

171 **3.1.2 Decision trees**

172 Decision Trees (DT) are basic estimators and non-parametric models used in Machine
 173 Learning. DT comprise two types of components: nodes and branches [66]. Each one of the data's
 174 features is examined at each node. For this reason, DT are flexible models that do not increase
 175 their number of parameters when adding more features. The internal nodes indicate an attribute
 176 test, and each branch and leaf represent the test result and the class tag, respectively. These nodes
 177 come in three different categories, and each one has a distinct geometric shape, such as a circle,
 178 rectangle, or triangle. DT is a simple ML learning model in term of interpretability and constitute
 179 the element piece of more advanced ensemble models described hereafter.

180 3.1.3 XGBoost

181 XGB is known as an upgraded gradient boosting machine implementation, that uses a more
 182 regularized model generation to control over-fitting more successfully using Friedman's gradient
 183 boosting method [67]. The prediction is made by using several additive functions:

$$Y_{ik} = Y_{ik+1} + \mu f_k \quad (1)$$

184 Where Y_{ik} is the predicted value of i th iteration, f_k is an estimator corresponding to a tree structure,
 185 Y_{i0} is the mean of predictions of training dataset, μ is the learning rate, facilitating steady model
 186 improvement while including new trees and preventing overfitting. It is important to remember that
 187 overfitting is the main issue with all ML models. At the k step, k th estimator is added to the model,
 188 and the estimation of Y_k can be done according to equation (2), f_k can be determined by minimizing
 189 the following objective function:

$$objective = \lambda T + \sum_{j=0}^T [E_j \omega + \frac{1}{2} (F_j + \gamma) w_j^2] \quad (2)$$

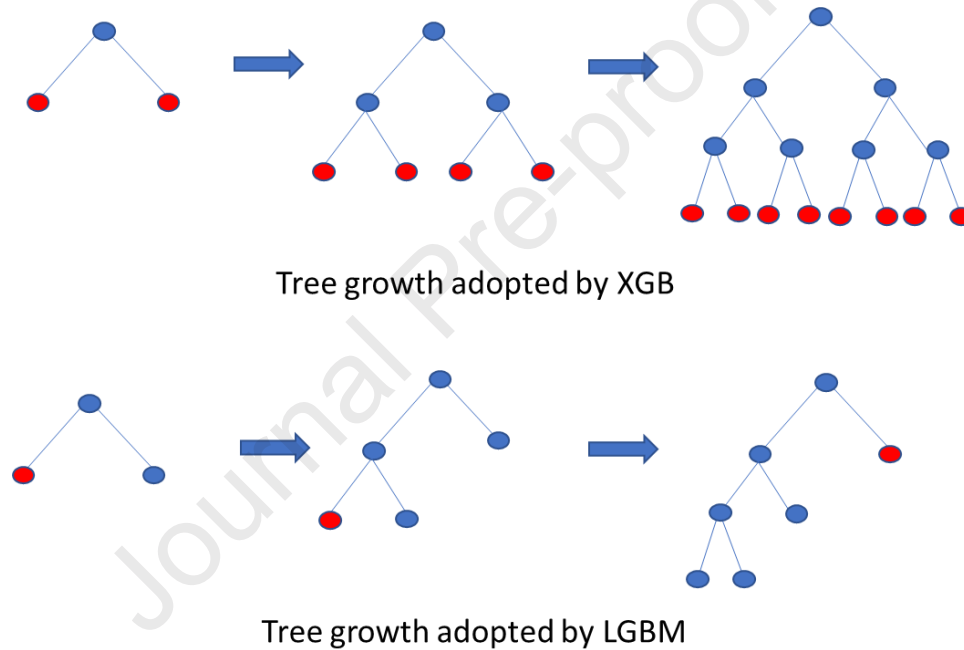
190 Where T represents the total number of leaves in the k th decision tree and w_j are the weights of
 191 each leaf. λ and γ are regularization parameters that control the simplicity of the tree structure to
 192 reduce overfitting. E_j and F_j are the sums of the samples associated with the j th leaf of the first and
 193 second gradients of the loss function, respectively.

194 3.1.4 Light Gradient Boosting (LGBM)

195 Light Gradient Boosting Machine (LGBM) is a new Gradient Boosted Decision Tree-based
 196 algorithm for machine learning [68]. It was originally introduced by Microsoft and is very similar

197 to XGB model. However, unlike most other implementations, LGBM does not grow a tree level-
 198 wise (row by row/horizontally). Instead, it implements the leaf-wise tree growth method (it grows
 199 vertically). This means that it selects the leaf that will have a maximum decrease in loss and grows
 200 on it. This building approach lowers the penalty for a wrong prediction. LGBM can also avoid
 201 over-fitting by limiting its tree depth. The main disadvantage of LGBM is that it covers many
 202 hyperparameters, making it harder to tune.

203 LGBM was created as a significant rival to XGBoost to increase training speed, use less
 204 memory, and retain excellent accuracy. The primary distinction between LGBM and XGBoost is
 205 how the trees are grown, as illustrated in Fig.3.



206
 207 **Fig. 3.** Different ways for growing trees between LGBM and XGB [69].

208 **3.2. Hyperparameters optimization**

209 A Bayesian-based hyperparameter optimization algorithm has been employed, namely the
 210 Tree-structured Parzen Estimator (TPE), which is a Sequential Model-Based Method [70]. The
 211 interest of TPE algorithm lies in its reduced runtime and the better scores of the optimized models
 212 on the final test set as compared to other optimization algorithms, especially Random Search or
 213 manually-based optimization. TPE algorithm can be briefly described as an exploration-
 214 exploitation algorithm that looks to optimize the expected improvement (EI) function, defined in
 215 eq. 12, at each iteration using a surrogate loss function and selecting the best couple of
 216 hyperparameters within a given search space.

$$EI_{y^*}(x) = \int_{-\infty}^{\infty} \max(y^* - y, 0) p(y|x) dy \quad (3)$$

217 Where y^* is a target performance, i.e. threshold value of the loss, e.g. objective, function, x is
 218 the proposed set of hyperparameters, y is the actual value of the loss using hyperparameters x , and
 219 $p(y | x)$ is the surrogate probability model expressing the probability of y given x . Maximizing the
 220 Expected Improvement with respect to x means finding the best hyperparameters under the
 221 surrogate function $p(y | x)$.

222 For TPE, $p(y | x)$ is approximated using Bayes' rule:

$$p(y|x) = \frac{p(x|y) \times p(y)}{p(x)} \quad (4)$$

223 Where $p(x|y)$, which is the probability of the hyperparameters given the score on the objective
 224 function, in turn, is expressed considering a split according to two different distributions for the
 225 hyperparameters: one where the value of the objective function is less than the threshold, $l(x)$, and
 226 one where the value of the objective function is greater than the threshold, $g(x)$:

$$p(x|y) = \begin{cases} l(x), & \text{if } y < y^* \\ g(x), & \text{if } y \geq y^* \end{cases} \quad (5)$$

227 The EI to maximize is then proportional to $g(x)/l(x)$ that is to be minimized:

$$EI_{y^*}(x) \propto \left(\gamma + \frac{g(x)}{l(x)} (1 - \gamma) \right)^{-1} \quad (6)$$

228 Where γ is the quantile of search result: $\gamma = p(y < y^*) = \int_{-\infty}^{y^*} p(y) dy$.

229 The hyperparameters search spaces of the four models used in this study are given in Table 2.

230

231 **Table 2.** Tuning ranges of hyperparameters.

LR	No hyperparameter				
DT	Max depth	Min samples	Min samples	Min weighted	
	[2, 100]	split	leaf	fraction at leaf node	
		[1, 30]	[1, 20]	[0, 0.5]	
XGB	Nb of trees	Learning rate	Max depth	Min child weight	Subsample ratio

	[10, 1000]	[0.005, 0.30]	[2, 100]	[1, 30]	[0.8, 1]
LGBM	Nb of trees	Learning rate	Max depth	Min child weight	Subsample ratio
	[10, 1000]	[0.005, 0.30]	[2, 100]	[1, 30]	[0.8, 1]

232 3.3. Results analysis

233 3.3.1 Performance evaluation

234 To calculate the scores of the models, three metrics indexes are used: mean absolute error (MAE),
235 coefficient of determination (R^2) and root mean square error (RMSE), which can be expressed as follows:

236 - Mean absolute error (MAE):

237 Mean absolute error is defined as the mean of differences between the predicted values and the
238 experimental values in the data, MAE is expressed as $MAE = \frac{1}{N} \sum |e_i - \hat{e}_i|$ where e_i is the value of
239 expansion of i-th point in the database, \hat{e}_i is the predicted value given by the models i-th sample point.

240 - Root mean square error (RMSE):

241 The error of a model in predicting quantitative data is often measured using the Root Mean Square Error

242 (RMSE). It is officially defined as $RMSE = \sqrt{\frac{1}{N} \sum (e_i - \hat{e}_i)^2}$

243 - Coefficient of determination (R^2)

244 The coefficient of determination is a statistical measurement that looks at how variations in one variable
245 may be explained by changes in a second variable. R^2 is expressed as $R^2 = 1 - \frac{\sum (e_i - \bar{e})^2}{\sum (e_i - \bar{e})^2}$ where \bar{e} is the
246 averaged value of expansion. Both MAE and RMSE can provide an accurate assessment of model
247 performance by clearly describing the residual error at each sample point. In contrast, R^2 creates a
248 dimensionless score that ranges from 0 to 1 by normalizing the squared residual error with the database
249 variance, in this study we worked with a logarithm of expansion, that is why the statistical indicators were
250 adapted to this transformation.

251 3.3.2 Model interpretation and features importance using SHAP

252 Although several ML-based investigations in solid materials have successfully predicted their
253 outputs with high accuracy, the interpretability of the ML models has received little attention.
254 SHAP reveals the underlying pattern that the database's EML models show, which can give a
255 thorough insight into the prediction of expansion behavior [71]. It is a means to determine how a

256 feature will affect the value of the target variable. The key idea is that the influence of features
257 depends on the full set of characteristics in the database rather than just one particular feature.
258 Therefore, SHAP retrains the model through all the combinations of features that contain the one
259 we are investigating to determine the influence of each feature on the expansion, an indicator of a
260 feature's significance is the average absolute magnitude of its effect on the output. The Shapley
261 value identifies the relative importance of each trait. The approach developed by SHAP for
262 comprehending model predictions may be used to understand even the most complex models.

263 **3.3.3 Prediction of time to reach specific expansions**

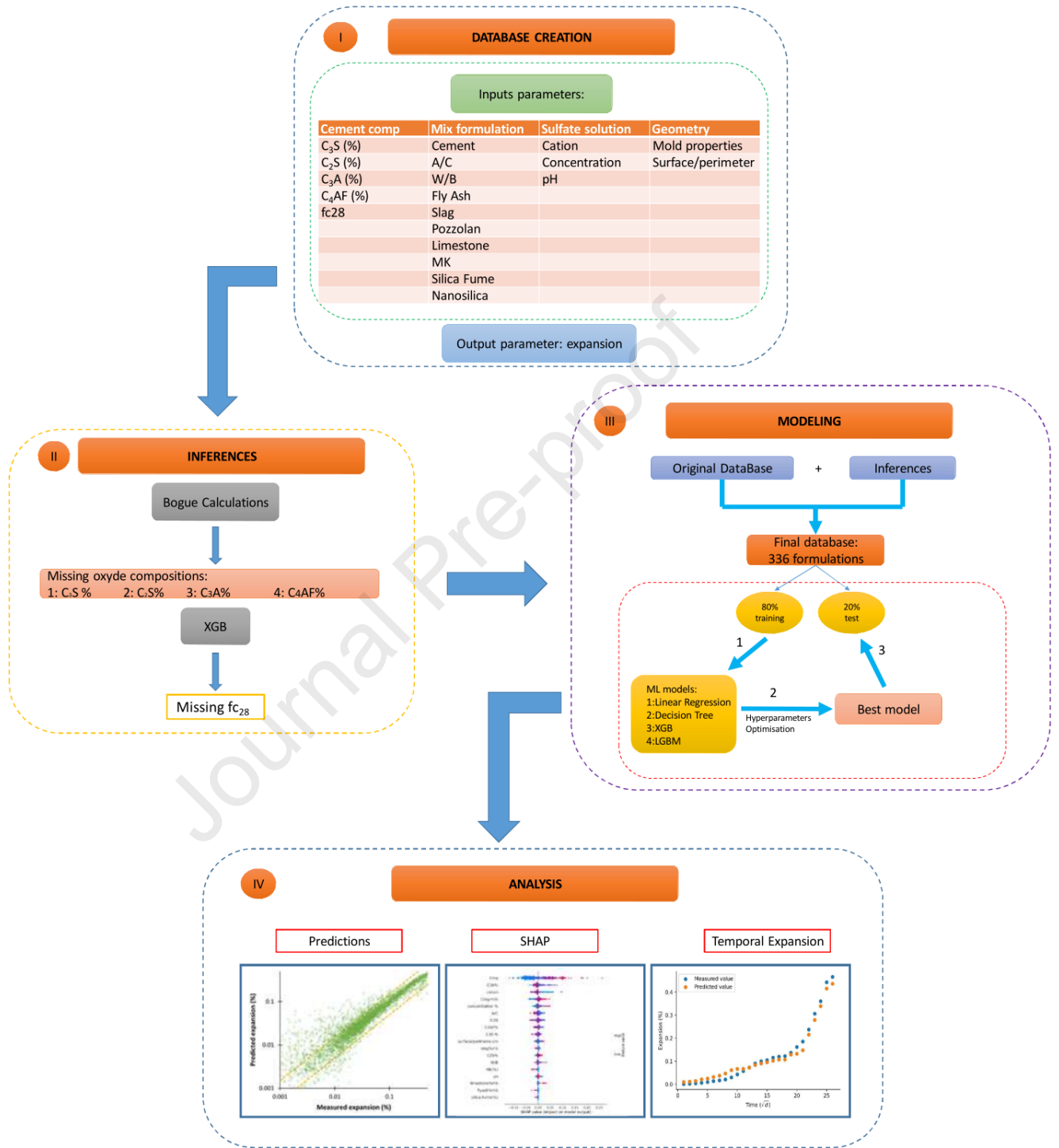
264 The time to reach 0.2% expansion was calculated with a $1\sqrt{d}$ precision for the test specimens
265 based on the model outputs to evaluate the model prediction capability, similar to experimentally-
266 measured time to failure [72]. For this purpose, the expansions of a given specimen were predicted
267 from 1 day to 1000 days using the optimized model. The time to reach 0.2% expansion was taken
268 as the first age at which the specimen's expansion reached this threshold value or a default value
269 of 1000 days if the threshold was not reached. Two cases could thus be distinguished: i) non-
270 sulfate-resistant cementitious materials that achieved an expansion higher than 0.2%. For these
271 samples, the ML models predicted time to reach this expansion was compared with the
272 experimental values; ii) sulfate-resistant cementitious materials. In this case, the default time of
273 1000 days was compared to the experimentally measured values, which were eventually set to
274 1000 days if no expansion had been observed.

275

276 **3.4. Methodology flowchart**

277 The investigation design is recapitulated in the methodology diagram presented in Fig. 4. Four
278 crucial steps, which have been previously described, can be highlighted: step (I) database creation
279 and description, step (II) predictions of fc28 and other missing values, step (III) selection of the
280 optimal ML model with the highest performance, and step (IV) expansion prediction and
281 sensitivity analysis using SHAP. Database creation was based on literature studies, 18 parameters
282 were selected as the model inputs, and the expansion was the output. In step II, fc28 prediction
283 was done to complete the database and prove the performance of chosen ML models. In step III,
284 the database is randomly split into 20% for testing and 80% for training. LR, DT, XGB, and LGBM
285 were trained, and their hyperparameters optimized. The performance of ML models was assessed
286 using R^2 , RMSE, and MAE. The best ML model was then used to predict concrete expansions,

287 and the influencing inputs on the output expansion were evaluated using SHAP.



288

289

Fig. 4. Methodology flowchart of the study

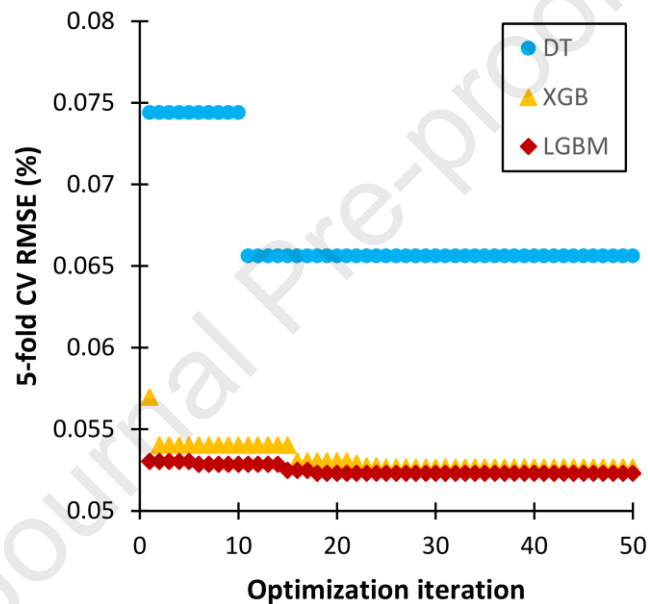
290

4. Results and discussion

291

4.1. Hyperparameters optimization

292 Tree-structured Parzen Estimator leads to a fast optimization hyperparameters tuning, as
 293 illustrated in Fig. 5. It can be seen from this figure that the algorithm RMSE on the five validation
 294 sets quickly decreased in around 20 iterations. The decrease in RMSE between the first model
 295 evaluated and the optimized model is around 0.001 for LGBM, 0.004 for XGB, and more than
 296 0.009 for DT model, highlighting the potential of this optimization procedure in this situation, in
 297 contrast with longer classical Bayesian optimizations and largely longer Random Search. The best
 298 mean result on the five validation sets after optimization has been obtained by the XGB model
 299 exhibiting an RMSE of 0.0515. The optimized hyperparameters of the DT, the XGB, and the
 300 LGBM models are reported in Table 3.



301
302 **Fig 5.** Optimization history using Tree-structure Parzen Estimator.

303

304 **Table 3.** Tunned hyperparameters of the ML models.

LR	No hyperparameter				
DT	Max depth	Min samples	Min samples	Min weighted fraction at	
	11	split	leaf	leaf node	
		6	13	0.02	
XGB	Nb of trees	Learning rate	Max depth	Min child weight	Subsample ratio
	200	0.08	52	28	0.841
LGBM	Nb of trees	Learning rate	Max depth	Min child weight	Subsample ratio
	590	0.215	41	29	0.973

305

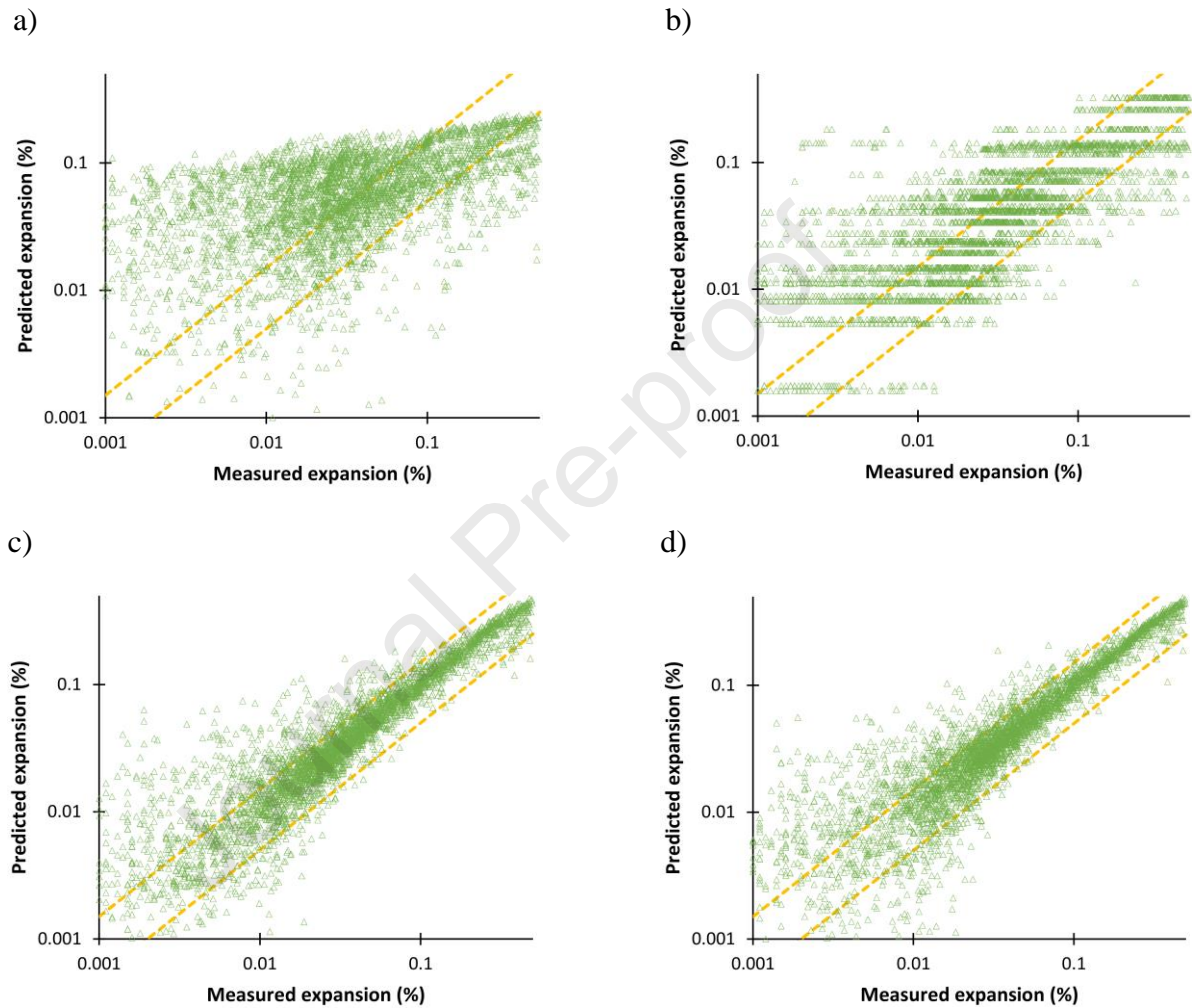
306 **4.2. Sulfate attack expansion predictions**

307 The prediction capacity of the optimized models on both the training and the test datasets are
308 illustrated in Fig. 6 and Fig. 7 resp. It can be observed that, after optimization, the models
309 performed well on the training set, especially for relatively large values of expansions higher than
310 0.05-0.1%. Though the LR model showed relatively poor performance in some cases, which can
311 be attributed to its low complexity, the other three models could provide predicted expansions
312 close to the measured values in most cases. Indeed, a high proportion of the predicted values lie
313 within a 50% interval compared to the experimentally measured values, as illustrated by the dashed
314 lines. This is a good result considering the relatively low precision of some reported results since
315 most of the studies generally aim to compare different mortar formulations with one non-sulfate
316 resistant formulation reducing the other samples' expansions resolution. Only a tiny number of
317 expansions higher than 0.2% were incorrectly predicted. These values, which are often associated
318 with formulations containing both SCM, represent a small proportion of the dataset due to the lack
319 of data in the literature. It is worth noting that these values can be either underestimated or
320 overestimated. The latter case is more favorable for building a secure model that might be looked
321 for in the future. Overall, from the graphs, it can be concluded that the LGBM and XGB models
322 performed the best on the training dataset, followed by DT model, while LR performed relatively
323 poorly.

324 The comparisons between the predicted and measured expansion values from the test set are
325 illustrated in Fig. 7. It can be observed that the predictions still match relatively well the
326 experimentally measured expansions in the case of entirely unknown samples. Based on the visual
327 spread of the predicted values, it can be concluded that XGB and LGBM models performed the
328 best. However, these models tend to slightly overestimate some values, especially for low
329 expansions.

330 Typical time evolutions of the expansions predicted by the optimized XGB are reported in
331 Fig. 8 and the corresponding mortar and concrete formulations from the test set are given in Table
332 4. As illustrated in all subfigures, and in agreement with the general results detailed in the
333 paragraph above, most predictions are close to the measured values, even in the case of irregular,
334 probably noisy, time evolutions. In most cases, the model was able to reproduce the two-stage
335 expansion with a limited expansion increase at the beginning, and then a sudden expansion

336 increase due to the formation of macro-cracks in the specimens. Moreover, the time to reach
 337 specific expansions such as 0.05% and 0.1% limit guidelines has been predicted with a relatively
 338 good precision of around $2 \text{ to } 3 \sqrt{\text{days}}$ in most cases. Some rare samples were incorrectly
 339 predicted as mentioned above, which opens rooms for improvement.



340 **Fig. 6.** Comparison between target and calculated outputs of the models on the training database:
 341 a) LR, b) DT, c) XGB, d) LGBM

342

343

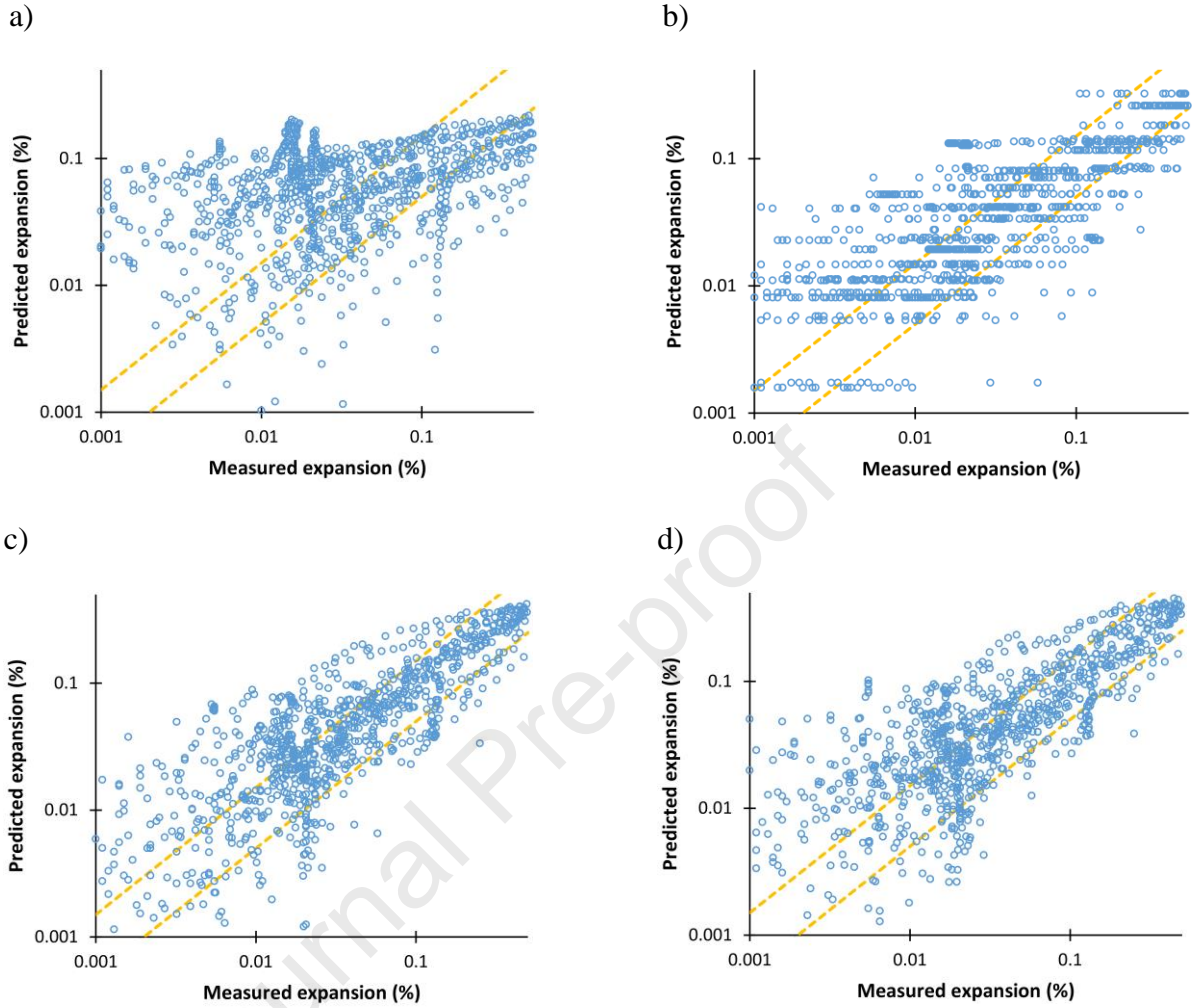
344

345

346

347

348



349 **Fig. 7.** Comparison between target and calculated outputs of the models on the testing database:

350 a) LR, b) DT, c) XGB, d) LGBM

351

352

353 **Table 4.** Mortar and concrete compositions of some typical test samples.

Ref	NSR-M [63]	SR-M [73]	NSR-C [54]	SR-C [8]
Type	CEM I	CEM I	CEM I	CEM I
C ₃ S %	56.6*	52.57	58.4	73.5
C ₂ S%	14.5*	18.11	14.65	5.5
C ₃ A%	5.7*	7.59	6.22	2
C ₄ AF%	12.1*	10.04	8.99	12.9
Cement(kg/m ³)	499	320	350	352
A/C	3.0	4.58	4.79	5.19
W/B	0.55	0.5	0.55	0.49
Fly Ash%	0	0	0	0

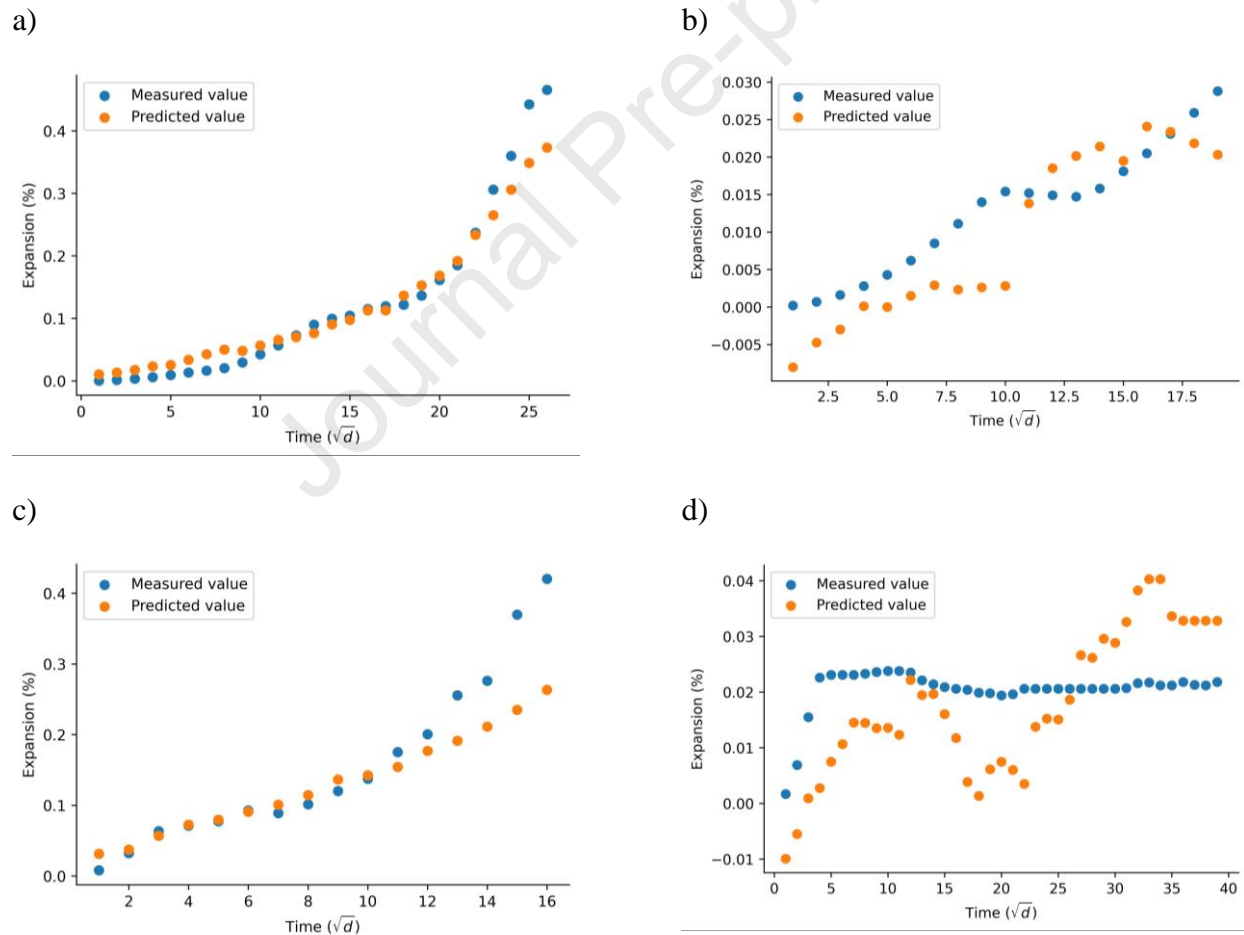
Slag%	0	40	0	0
Limestone%	0	0	0	0
MK (%)	0	0	0	0
Silica Fume (%)	0	0	0	0
Cation	Mg	Na	Na	Na
Concentration %	4.24	5	5	0.3
pH	7	10***	10***	7.5
Mold properties	prismatic	prismatic	cylindrical	prismatic
Surface/perimeter cm	1	1	2.5	1.75
fc28 (MPa)	46.1**	48.5**	43.1	52.7**

354 * Calculated using Bogue calculation

355 ** Inferred using the dedicated XGB model (cf section 2.2.1)

356 *** Imputed (cf section 2.2.2)

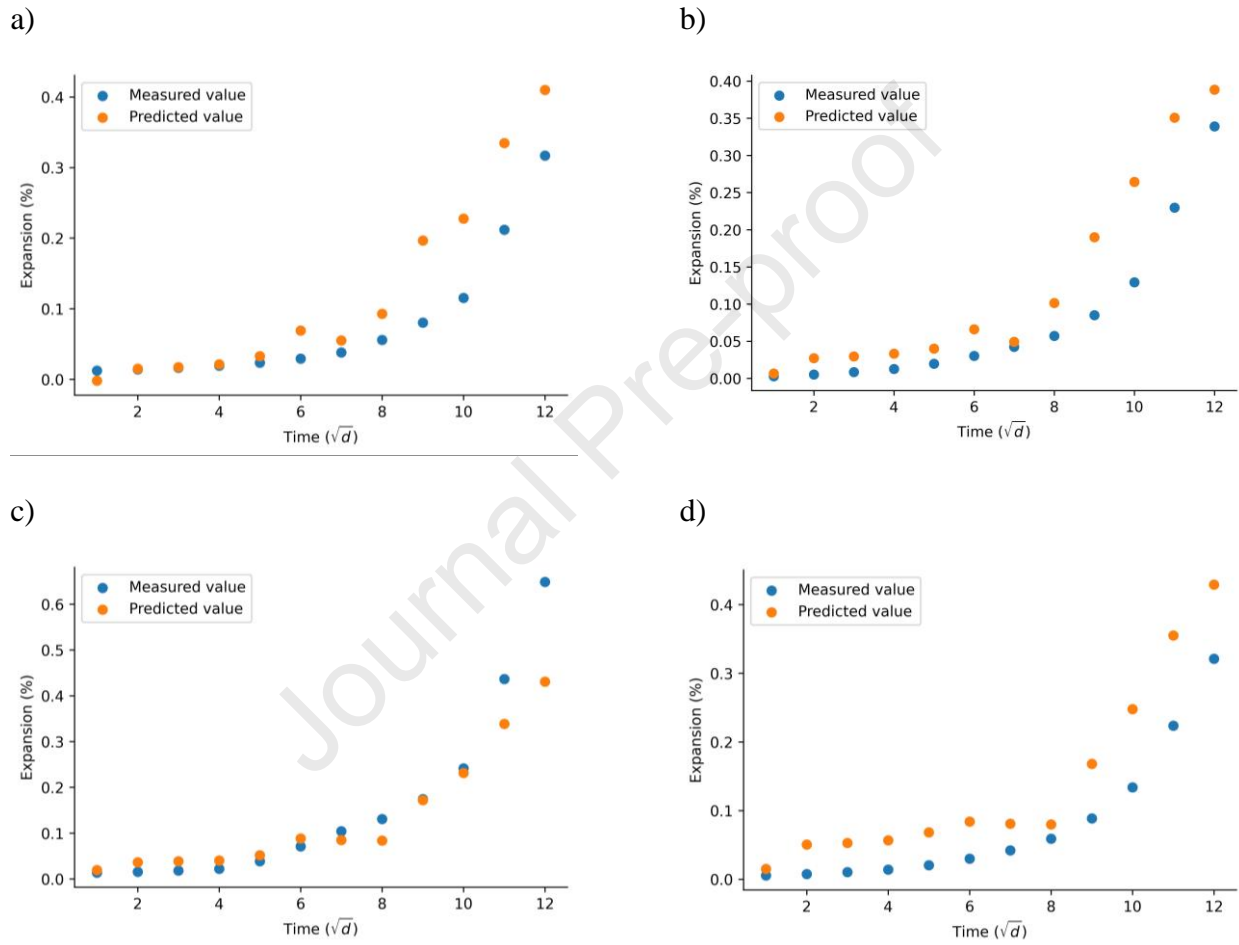
357



358 **Fig 8.** Typical predictions of expansion evolution of mortar and concrete samples due to external sulfate
 359 attack: a) non sulfate resistant mortar (NSR-M), b) sulfate resistant mortar (SR-M), c) non sulfate
 360 resistant concrete (NSR-C), d) sulfate resistant concrete (SR-C).

361 4.3. Model universality

362 The universality, i.e. generalization capacity of the model was further validated by predicting
 363 the expansion of samples from a study not included in the database [74]. The comparison of
 364 measured and predicted values shown in Figure 9 confirms the good generalization capacity of the
 365 model, as all four expansion kinetics were correctly reproduced. Additionally, predictions of
 366 sulfate-resistant mixtures from this study were also satisfactorily predicted.



367 **Fig 9.** Model universality test: expansion predictions of four samples from a study not included in the
 368 database.

369 4.4. Optimized models' performances

370 The performance of the optimized models on the training and the test sets has then been
 371 evaluated by comparing the predicted to the interpolated measured expansions relatively to the
 372 square root of time. The mean values of the performance predictions of the models have been
 373 reported in Table 5. As illustrated by the table, the best results have been obtained by the ensemble

374 models, e.g., XGB and LGBM. Indeed, the best results on the training set have been obtained by
 375 the LGBM model with mean R^2 values of 0.947 and a corresponding RMSE value of 0.0205. This
 376 model can very well learn the mechanisms at the origin of expansion. XGB model also performed
 377 very well on the training set with R^2 and RMSE values of 0.933 and 0.0230 resp. The other models,
 378 LR and DT, were found to be less performant with R^2 values of 0.358 and 0.591 resp., which agrees
 379 with the literature relative to the prediction of concrete properties using Machine Learning. This
 380 observation can be attributed to the lower complexity of these models, which is insufficient to
 381 efficiently learn the hidden patterns underlying the external sulfate attack expansion.

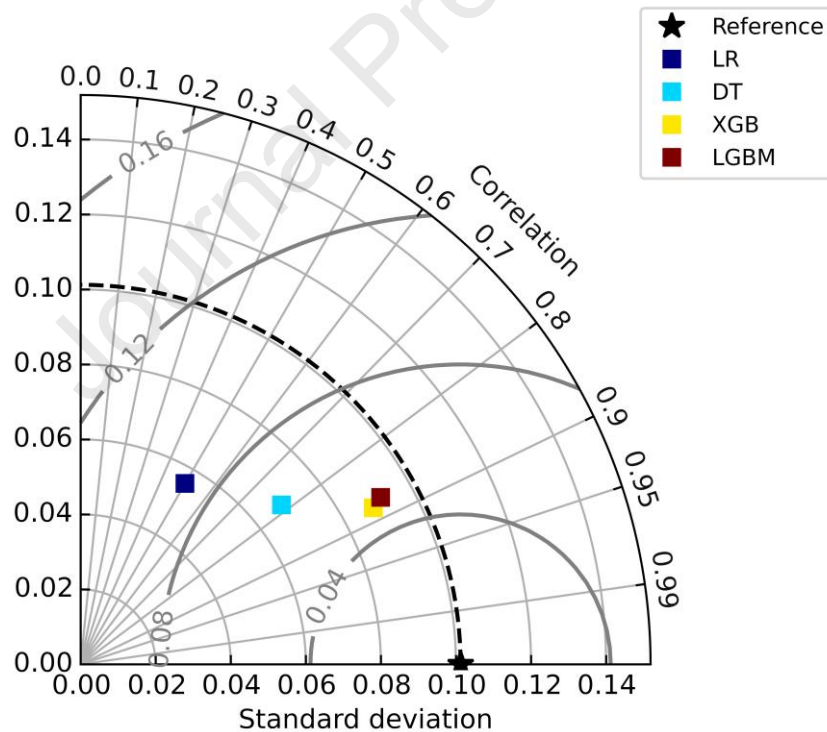
382 The generalization capacity of the models and their performance on unknown data has been
 383 assessed by predicting the test data, that is, full expansion curves knowing only cement
 384 composition, mortar composition, specimens' geometry, and sulfate solution characteristics. As
 385 illustrated in Fig. 7 and Table 5, the XGB model obtained the best results on the test set. R^2 , RMSE
 386 and MAE values of 0.788, 0.0466%, and 0.0273% were achieved resp. LGBM model performed
 387 slightly worse with R^2 , RMSE and MAE values of 0.762, 0.0495%, and 0.0307% resp. Again, LR
 388 and DT models performed significantly worse, which agrees with the abovementioned
 389 observations made on the training set results. Though these values are slightly lower than the scores
 390 on the training set, which can be explained by the difficult and highly nonlinear problem and the
 391 relatively limited amount of data sources, these values can be acceptable to achieve good
 392 predictions and parameters interpretation, as we will see in the next sections.

393 **Table 5.** Mean machine learning algorithms performance for external sulfate attack expansion
 394 prediction.

Algorithm	Training set			Test set		
	R^2	RMSE (%)	MAE (%)	R^2	RMSE (%)	MAE (%)
LR	0.358	0.0714	0.0465	0.240	0.0882	0.0595
DT	0.591	0.0570	0.0306	0.596	0.0642	0.0375
XGB	0.933	0.0230	0.0112	0.788	0.0466	0.0273
LGBM	0.947	0.0205	0.0110	0.762	0.0493	0.0307

395 An overall evaluation of the models can be visualized using a Taylor diagram, as illustrated
 396 in Fig. 10, which summarizes three valuable characteristics of the models compared to the
 397 measured values: the standard deviation associated with the model's predictions, the correlation

398 between the predictions and the experimental values, and the centered root-mean-square difference
 399 (RMSD). Similarly to what has been reported previously concerning RMSE, the best RMSD has
 400 been obtained by the LGBM model, followed by XGB, DT, and LR models. Concerning the
 401 correlation of the models with the experimental values, the best correlation is obtained by the
 402 LGBM and XGB models with values around 0.86 and 0.88 resp. Though XGB performed better
 403 regarding RMSD and correlation, the standard deviation of the experimental data of around 0.1%
 404 is almost reproduced by the LGBM model, which is probably due to the highest number of trees
 405 composing the optimized model (see Table 3). However, the standard deviations associated with
 406 the two other models are significantly smaller than the experimental value, which confirms the
 407 difficulty of DT and LR models in grasping the experimental data diversity. For this reason, it can
 408 be concluded that XGB is the best model per se on the test data in this study, but the LGBM model
 409 is more complex due to a higher number of trees. Thus, the optimized XGB model results will be
 410 discussed in the following sections related to the model interpretation.



411
 412 **Fig. 10.** Taylor diagram representing ML models performance on the test set.

413

414 **4.5. Model interpretation and feature importance analysis using Shapley Additive Explanations**

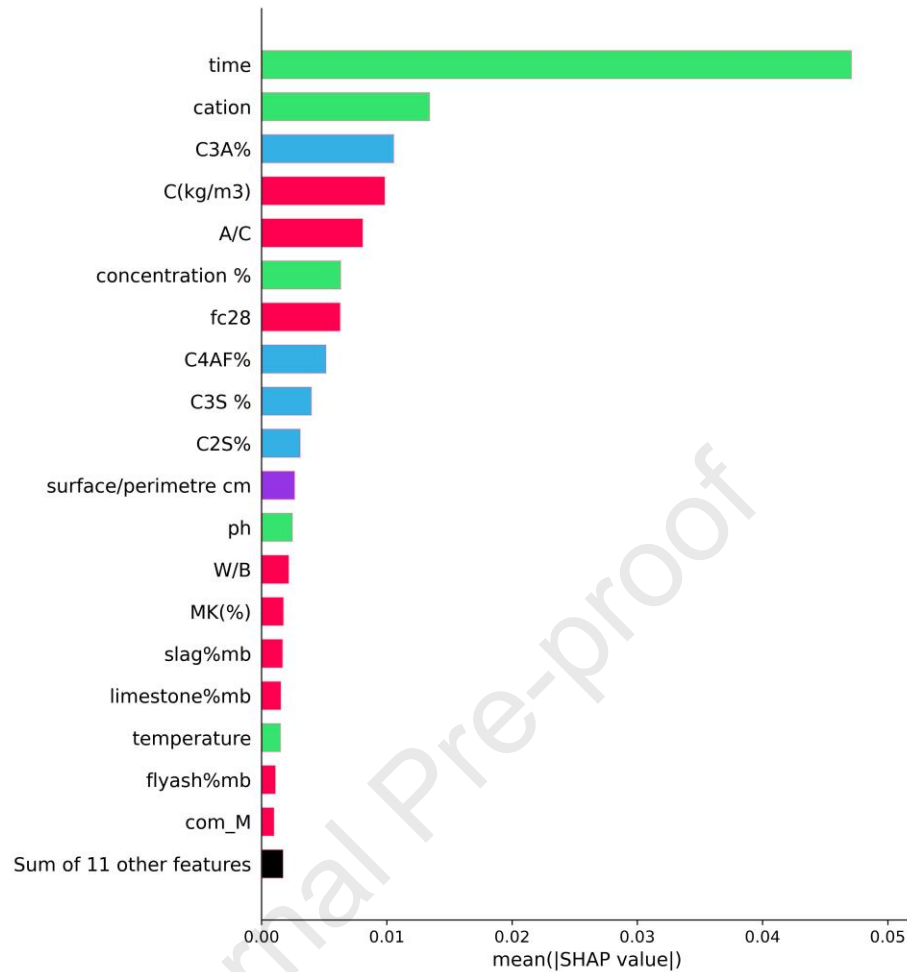
415 **(SHAP)**

416 **4.5.1. Global interpretation**

417 The most influential features on the expansion predictions have been obtained using SHAP,
418 and the global SHAP values are reported in Fig. 11. In this figure, the features are classified in
419 descending order based on their influence from top to bottom and colored depending on their type.
420 Notably, the top 18 parameters accounted for 98.5% of the cumulative mean absolute SHAP value.
421 Excluding time, the respective contributions of clinker composition, mix proportion, sample
422 geometry, and sulfate solution characteristics are 34%, 36%, 3%, and 27%, illustrating the intricate
423 nature of the ESA mechanism and the need to construct intricate databases to effectively utilize
424 ML models to anticipate ESA-induced expansion.

425 According to the model, the cation type, sodium or magnesium, is the most influential
426 parameter, besides time. While additional studies exploring magnesium would have been
427 advantageous, this finding aligns with existing literature. While Na^+ has no influence on the attack
428 mechanism, Mg^{2+} ions from MgSO_4 react with cement paste hydrates and prevail over sulfate
429 attack. The most significant consequence of MgSO_4 is the formation of M-S-H in place of C-S-H.
430 As M-S-H do not provide the same cohesive characteristics as C-S-H, the cementitious sample
431 will lose compressive strength over expansion [75].

432 Among the most influential parameters predicted by the model, the water and cement content,
433 C_3A content, and sulfate solution concentration have already been extensively documented and are
434 already taken into account in various standard recommendations. The model reveals 28-day
435 compressive strength as another influential parameter. Strength is commonly used as a degradation
436 indicator more than a parameter [76–78]. This result is related to porosity: a sample with high
437 porosity is prone to sulfate ingress and, simultaneously, has less compressive strength. Finally,
438 time of exposure is the most influential parameter. It is worth noting that among these most
439 influential parameters, various types of parameters, e.g., cement composition, mixture proportions,
440 and sulfate solution characteristics are all present, which highlights the complexity of the sulfate
441 attack degradation.



442

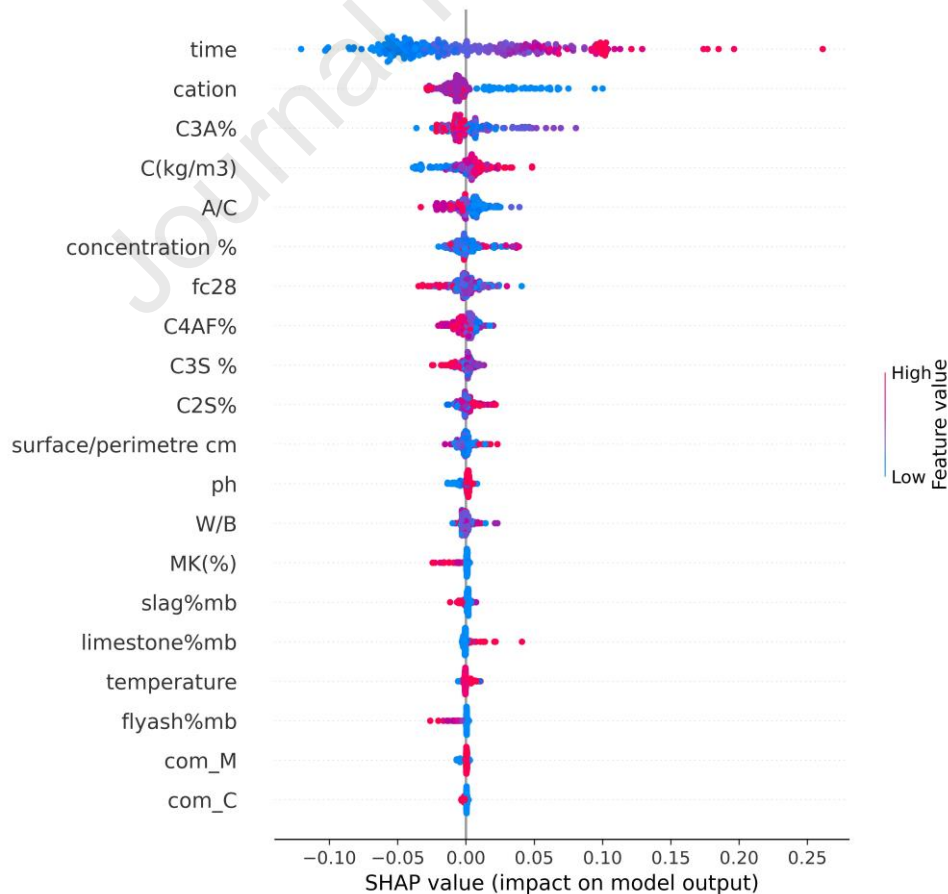
443 **Fig 11.** Feature importance plot of the optimized XGB model (clinker parameters, mix factors, sample
 444 geometry-related parameters and environmental factors are colored in blue, red, purple and green resp.)

445 From the SHAP summary plot illustrated in Fig. 12, the relative influence of the most
 446 influential parameters can be qualitatively determined using the spread of the dots and their color.
 447 It has been found that increasing water and cement contents generally increase the expansion.
 448 Increasing C_3A content also increases the expansion, especially when transitioning from very low
 449 C_3A content close to 0% to moderate C_3A content of around 7-8%. Regarding the other factors
 450 related to clinker composition, it was found that the C_4AF content is the second most important
 451 clinker factor, the higher its concentration the lower the expansion. This can be partly explained
 452 by its negative correlation with C_3A content, as illustrated in Fig. 2. C_3S and C_2S contents have a
 453 relatively small influence on the expansion. Fig. 12 also shows that an increase in 28-day
 454 compressive strength leads to a decrease in sulfate expansion, while higher aggregate-to-cement
 455 ratios are associated with smaller expansions, which can be explained by the fact that only the

456 cement paste reacts.

457 Though significantly less important according to the SHAP analysis, the influence of SCM
 458 can also be quantified and agreed with the literature [79–82]. Based on the model results, it has
 459 been found that limestone can harm sulfate resistance at high dosage, while calcined clay and slag
 460 addition have a powerfully positive impact on sulfate resistance, and fly ash has a relatively smaller
 461 yet positive influence on sulfate resistance. Conversely, silica fume addition might negatively
 462 influence sulfate attack resistance, especially for moderate to high dosages.

463 Among the specimen geometrical parameters, it has been found that the surface-to-perimeter
 464 ratio has the most substantial influence, which agrees with the experimental observations [83,84].
 465 Indeed, the higher the surface-to-perimeter, the smaller the expansion. Other geometrical
 466 parameters such as the specimen shape (mold properties) and height have a smaller influence,
 467 though quantitatively close to some SCM additions. Thus, the model results support the
 468 development of accelerated tests involving specimens with small sections. Additionally, a careful
 469 analysis of the sulfate induced expansion results must be performed regarding these parameters.



471 **Fig 12.** SHAP summary plot of the optimized XGB model.
472

473 **4.5.2 Feature dependence plots**

474 The feature dependency of the results has been analyzed in detail using the SHAP feature
475 dependence plots. As illustrated in the dependence plots reported in Fig. 13, the relative influence
476 of each parameter on the computed SHAP values and, therefore, their influence on the predicted
477 expansion can be calculated. Apart from the cation type of the sulfate solution, which greatly
478 influences the development of expansion, as explained in the previous section, the most influential
479 parameters belong to the cement composition and the mixture proportion. Among these
480 parameters, cement content and water content, which is not reported, have a similar effect and
481 strongly and almost linearly influence the expansion as illustrated in Fig. 13 a). Indeed a difference
482 in SHAP values of around 0.05% is almost systematically observed between mixes with cement
483 contents around 100 kg/m³ and mixes with more than 500 kg / m³ of cement. Similarly, as
484 illustrated in Fig. 13 b), SHAP values increase around 0.1% when C₃A content increases from
485 around 0% to 8%, meaning that higher expansions are associated to C₃A contents of around 8% as
486 compared to smaller to C₃A contents. However, higher C₃A contents (<8%) have a smaller
487 influence on SHAP value (around 0%). Even though this result might be due to the relatively small
488 number of high-C₃A content cements in the database, this could also be explained by the fact that
489 other factors predominate in the expansion phenomenon of these specific concretes.

490 Mixtures characteristics such as the 28-day compressive strength and the aggregate-to-cement
491 ratios clearly influence the expansion values. As illustrated in Fig. 13 c), the SHAP values
492 associated with high 28-day compressive strength values decrease. In the same way, increasing the
493 A/C ratio reduces the predicted expansion, especially when the A/C ratio increases from around 1-
494 2 to 4-5.

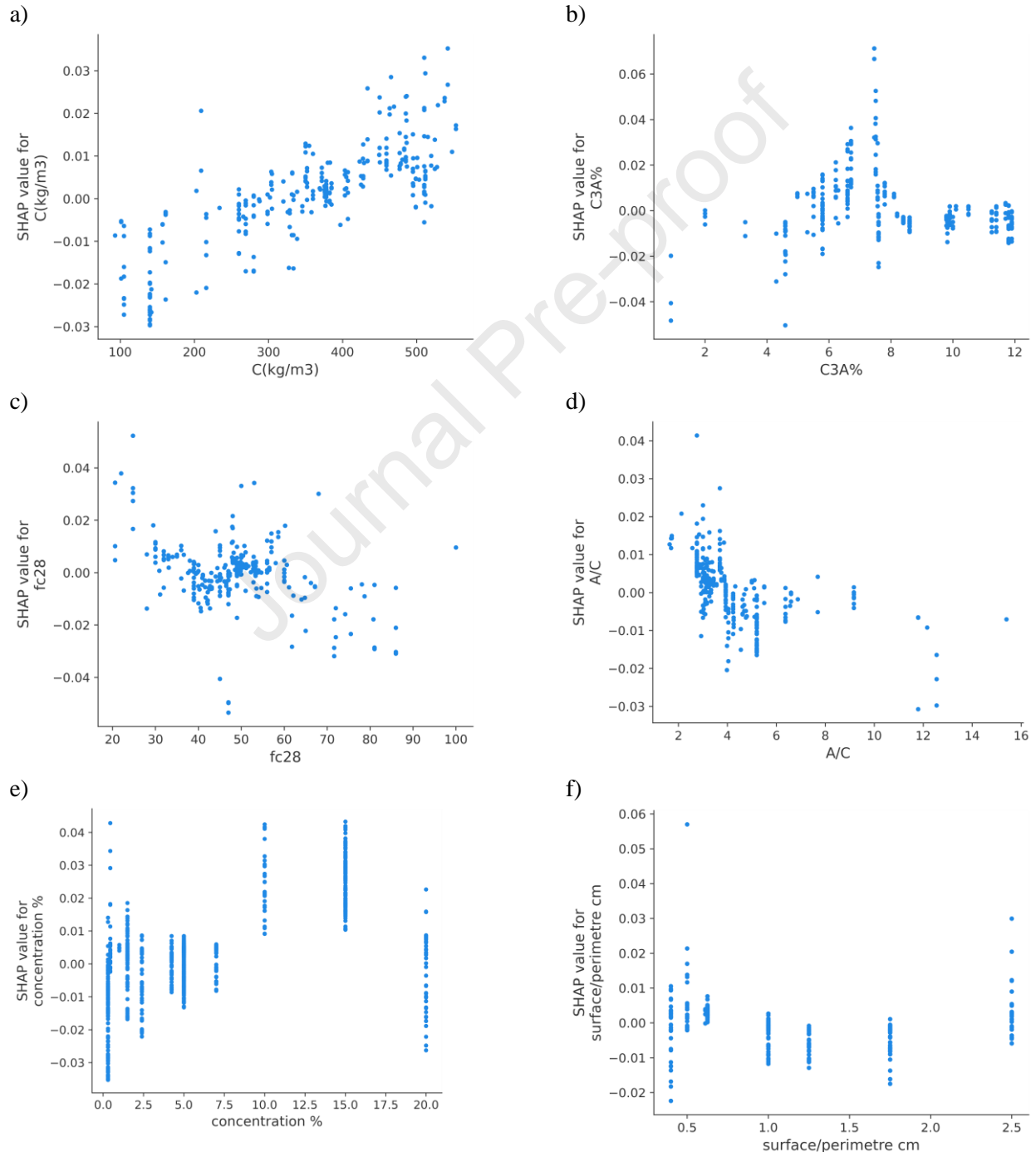
495 Accelerated test conditions such as sulfate solution concentration and geometrical properties
496 of the samples can be analyzed thoroughly. As illustrated in Fig. 13 e), increasing sulfate
497 concentration values, in the range of 0% to 15%, generate more expansion. However, sulfate
498 concentrations around 20% might not accelerate the degradation. Similarly, when the surface-to-
499 perimeter ratio of the specimens increases from around 0.5 to 1.7, SHAP values decrease, which
500 means that the samples are less prone to sulfate expansion.

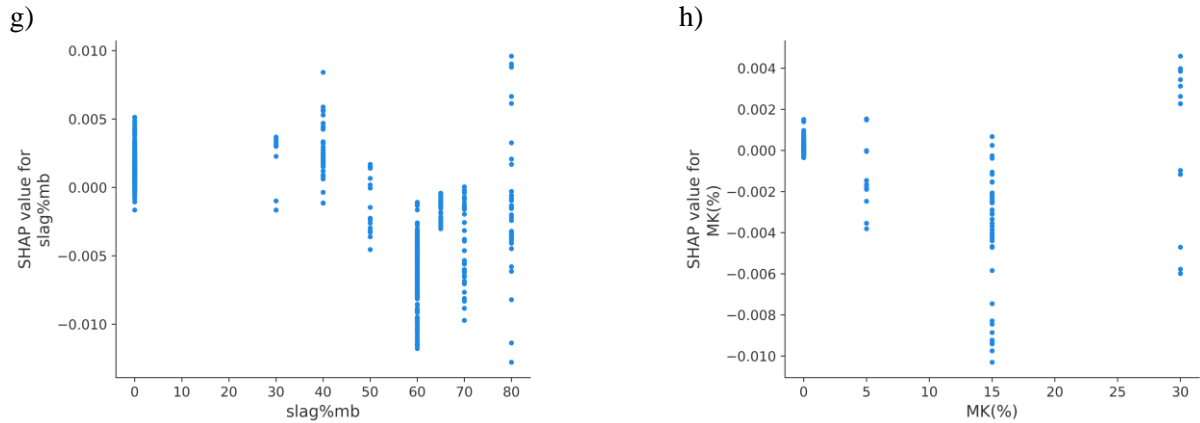
501 The partial substitution of cement by SCM can also be analyzed though more data would be

502 welcome. As illustrated in Fig. 13 g), cement replacement by slag generally leads to lower
503 expansions, especially for replacement rates higher than 30-40% [17,85]. In the same way, cement
504 replacement by calcined clay usually decreases expansions, although 30% replacement rates might
505 not always have positive effects.

506

507





508 **Fig 13.** SHAP feature dependence plot: a) C₃A, b) cement content, c) fc28, d) A/C, e) sulfate
 509 concentration, f) surface over perimeter, g) slag content, and, h) calcined clay content.

510

511 4.5.3. Local interpretation

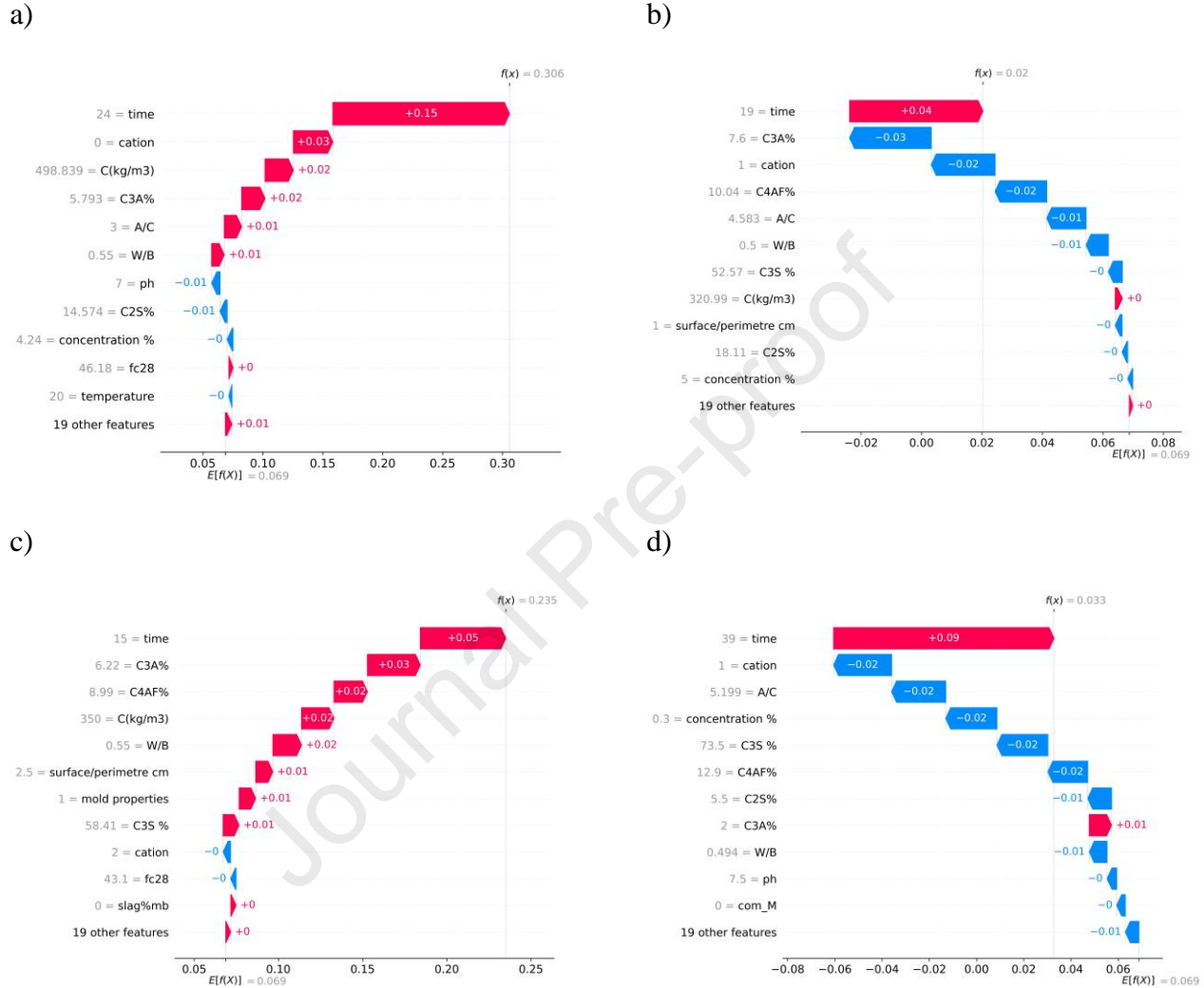
512 The local SHAP analysis of four typical mortar and concrete samples whose composition is
 513 given in Table 4 are reported in Fig. 14. With a fixed base value of 0.069%, the final prediction
 514 for expansion, displayed atop each graph, is the counteracting result of SHAP values of different
 515 features.

516 According to the SHAP analysis of the results concerning mortar samples (Fig. 14 a and b),
 517 the amount of cement has a negative impact on the expansion results. Thus, mortar samples made
 518 with cement containing 5.8 % of C₃A can have more expansion than mortar samples made with
 519 7.6 % of C₃A. This indicates that the C₃A content can represent a limit between SR and NSR
 520 cement. However, above this limit there is no proportionality between expansion and C₃A content
 521 [86]. Moreover, other parameters can compensate the poor performance of a given cement such as
 522 the low cement content, a relatively high aggregate-to-cement ratio or a moderate water-to-binder
 523 ratio, as in sample SR-M (Fig 14 b).

524 The SHAP local analysis also gives consistent and valuable indications for NSR-C and SR-C
 525 concrete specimens qualification, as illustrated in Fig. 14 c) and d) resp. The C₃A content of the
 526 clinker part is the parameter that has the most negative impact on the expansion for NSR-C. The
 527 concrete samples made with cement containing an important proportion of C₃A must present assets
 528 to offset the great reactivity of the cement to sulfate ions. It can be a lower cement content or a low
 529 w/b ratio. Here it is not the case for the NSR-C concrete, as the high cement content and w/b ratio
 530 have, associated with a low aggregate-to-cement ratio, favor expansion. Conversely, in SR-C
 531 sample, the formulation of concrete, the cement composition and the conditions of exposure

532 decrease the expansion due to the reaction to sulfate. Those parameters compensate for the slightly
 533 negative effect of the 2% C₃A content.

534



535 **Fig 14.** Local interpretation of mortar and concrete samples expansion due to external sulfate attack: a)
 536 non sulfate resistant mortar (NSR-M), b) sulfate resistant mortar (SR-M), c) non sulfate resistant concrete
 537 (NSR-C), d) sulfate resistant concrete (SR-C).

538

539 **Table 6.** Comparison of measured and predicted expansions of typical test samples.

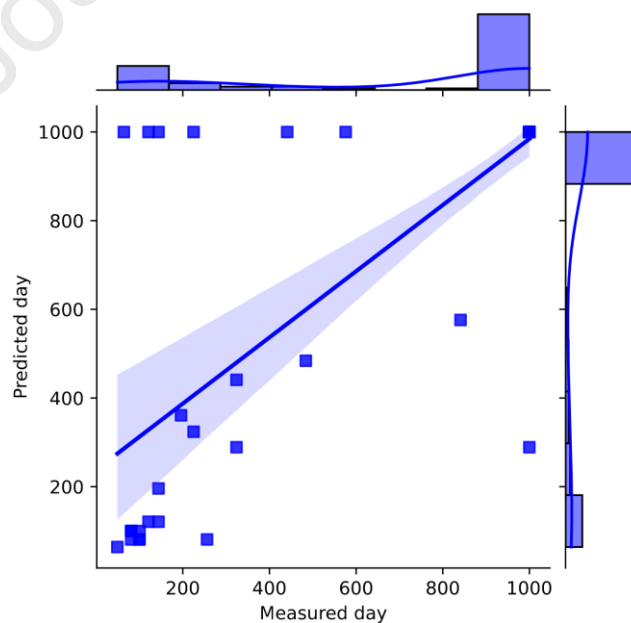
Ref	NSR-M [63]	SR-M [87]	NSR-C [54]	SR-C [8]
Time (days)	576	361	225	1521
Measured expansion (%)	0.360	0.029	0.369	0.022

Predicted expansion (%)	0.306	0.020	0.235	0.033
-------------------------	-------	-------	-------	-------

540

541 4.6. Prediction of time to reach specific expansions

542 The time to reach 0.2% expansion of the test specimens has been calculated following the
 543 methodology that has been aforementioned. The results are represented in Fig. 15. It can be
 544 observed in this figure that among the 68 samples, 43 were correctly predicted to not reach 0.2%
 545 expansion (points with x and y values equal to 1000 days on the top right), 18 samples showing an
 546 extension have been very well predicted (bottom-left part of the graph), while 7 samples, i.e. 10%,
 547 expansion time have been incorrectly predicted (6 samples have been underestimated and 1
 548 samples have been overestimated). In total, in 84% of the cases, the prediction and measured time
 549 differed less than 100 days. The R^2 and correlation values between the predicted and
 550 experimentally measured expansion time reached 0.64 and 0.80 resp., and the regression line and
 551 95% confidence interval reported on the graph can be used to practically infer the time t_i reach a
 552 specific expansion. Therefore, it can be concluded that, even though some improvements may be
 553 needed to precisely predict the time to reach a given expansion, the optimized Ensemble Machine
 554 Learning models can be advantageously employed to estimate the degradation time of mortar and
 555 concrete specimens subjected to accelerated external sulfate attack degradation tests and can help
 556 select non-expansive formulations.



557

558 **Fig 15.** Comparison of XGB predicted and measured time needed to reach a 0.2% expansion with

559 regression line and 95% confidence interval (1000d values are attributed to specimens not reaching the
560 0.2% expansion threshold)

561 **5. Conclusions and perspectives**

562 This study investigated the potential of machine learning models to predict the expansion of
563 cementitious materials incorporating supplementary cementitious materials (SCM) subjected to
564 external sulfate attack (ESA) degradation. For the first time, a comprehensive database
565 documenting the expansion of mortar and concrete specimens has been built. Various types of
566 inputs have been considered: cement composition, mixture proportions, sulfate solution
567 characteristics, and geometrical features of the samples. Several techniques have been developed
568 to fill in the missing values, such as using an XGB model to infer the missing 28-day compressive
569 strengths. Then four machine learning (ML) models of ascending intricacy were used to predict
570 the temporal evolution of expansion. The machine learning models have been optimized using the
571 Tree-structured Parzen Estimator algorithm. Next, Shapley Additives Explanations (SHAP) were
572 then used to interpret the machine learning models' performances, and the time to reach specific
573 expansion were calculated using the test predictions. The results were discussed and compared to
574 the literature, demonstrating the ability of ensemble ML models to predict ESA-induced
575 expansion. The following main conclusions can be drawn:

- 576 - ML models can be applied to predict ESA-induced expansion thanks to a comprehensive
577 database gathering from the literature 336 conventional, binary and ternary mortar and
578 concrete sample expansions with 20 parameters. Expansion values have been interpolated,
579 and values higher than 0.5% have been filtered out to finally generate a database
580 containing 5294 expansion values at different times.
- 581 - Two ensemble machine learning models, Light Gradient Boosting (LGBM) and Extreme
582 Gradient Boosting (XGB), were trained on the completed database using a 5-fold CV
583 procedure after using a train-test split on samples, and outperformed the other two models
584 under investigation. The best optimized XGB model achieved a good R^2 accuracy of 0.933
585 and 0.788 on the training and the test set resp. Its universality has been validated on
586 unknown data.
- 587 - The most influential parameters were the cation type in the sulfate solution, the water and
588 cement contents in the mixture, the C_3A amount within the cement, the 28-day

589 compressive strength (which serves as a porosity indicator), the sulfate solution
590 concentration, and the aggregate-to-cement ratio. The clinker composition, the mix
591 proportion, the geometry of the sample, and the quantity of sulfate solution contributed
592 34%, 36%, 3%, and 27%, respectively, demonstrating the complex nature of ESA.

593 - An in-depth analysis of some predicted expansions from specimens in the test set ensured
594 the consistency of the model and helped quantify the impact of the input parameters in
595 these specific cases.

596 - Time to reach specific expansions due to ESA can be estimated using ML models. In 84%
597 of the cases, the predicted and measured time for specimens from the test set to reach a
598 0.2% expansion differed less than 100 days.

599 The study might open up new research paths related to the design of cementitious materials
600 with SCM that can resist the external sulfate attack. Moreover, this model could help develop more
601 efficient accelerated tests to assess the sulfate resistance of cementitious materials quickly. Such
602 advanced models might be of interest in the future regarding highly durable eco-friendly
603 cementitious materials development.

604

605 **Conflict of Interest:** The authors declare that there is no conflict of interest.

606

607 **Funding:** This research did not receive any specific grant from funding agencies in the public,
608 commercial, or not-for-profit sectors.

609

610 **Availability of data and material:** Data will be provided upon request.

611

612 References

- 613 [1] B.A. Clark, P.W. Brown, Phases formed during hydration of tetracalcium aluminoferrite in 1.0M magnesium
614 sulfate solutions, *Cement and Concrete Composites*. 24 (2002) 331–338. [https://doi.org/10.1016/S0958-](https://doi.org/10.1016/S0958-9465(01)00084-1)
615 [9465\(01\)00084-1](https://doi.org/10.1016/S0958-9465(01)00084-1).
- 616 [2] X. Ping, J.J. Beaudoin, MECHANISM OF SULPHATE EXPANSION, 22 (n.d.) 10.
- 617 [3] C. Yu, W. Sun, K. Scrivener, Mechanism of expansion of mortars immersed in sodium sulfate solutions,
618 *Cement and Concrete Research*. 43 (2013) 105–111. <https://doi.org/10.1016/j.cemconres.2012.10.001>.
- 619 [4] W. Müllauer, R.E. Beddoe, D. Heinz, Sulfate attack expansion mechanisms, *Cement and Concrete Research*.
620 52 (2013) 208–215. <https://doi.org/10.1016/j.cemconres.2013.07.005>.

- 621 [5] Z. Makhloufi, S. Aggoun, B. Benabed, E.H. Kadri, M.Bederina, Effect of magnesium sulfate on the
622 durability of limestone mortars based on quaternary blended cements, *Cement and Concrete Composites*. 65
623 (2016) 186–199. <https://doi.org/10.1016/j.cemconcomp.2015.10.020>.
- 624 [6] D. Damidot, S.J. Barnett, F.P. Glasser, D.E. Macphee, Investigation of the $\text{CaO}-\text{Al}_2\text{O}_3-\text{SiO}_2-\text{CaSO}_4-\text{CaCO}_3-\text{H}_2\text{O}$ system at 25°C by thermodynamic calculation, *Advances in Cement Research*. 16
625 (2004) 69–76. <https://doi.org/10.1680/adcr.2004.16.2.69>.
- 626 [7] F. Bellmann, B. Möser, J. Stark, Influence of sulfate solution concentration on the formation of gypsum in
627 sulfate resistance test specimen, *Cement and Concrete Research*. 36 (2006) 358–363.
628 <https://doi.org/10.1016/j.cemconres.2005.04.006>.
- 629 [8] R. El-Hachem, E. Rozière, F. Grondin, A. Loukili, New procedure to investigate external sulphate attack on
630 cementitious materials, *Cement and Concrete Composites*. 34 (2012) 357–364. <https://doi.org/10/fggr6x>.
- 631 [9] D. Planel, J. Sercombe, P. Le Bescop, F. Adenot, J.-M. Torrenti, Long-term performance of cement paste
632 during combined calcium leaching–sulfate attack: kinetics and size effect, *Cement and Concrete Research*.
633 36 (2006) 137–143. <https://doi.org/10.1016/j.cemconres.2004.07.039>.
- 634 [10] J. Bizzozero, C. Gosselin, K.L. Scrivener, Expansion mechanisms in calcium aluminate and sulfoaluminate
635 systems with calcium sulfate, *Cement and Concrete Research*. 56 (2014) 190–202.
636 <https://doi.org/10.1016/j.cemconres.2013.11.011>.
- 637 [11] N.J. Crammond, The thaumasite form of sulfate attack in the UK, *Cement and Concrete Composites*. 25
638 (2003) 809–818. [https://doi.org/10.1016/S0958-9465\(03\)00106-9](https://doi.org/10.1016/S0958-9465(03)00106-9).
- 639 [12] NF EN 197-1.pdf, (n.d.).
- 640 [13] H.T. Cao, L. Bucea, A. Ray, S. Yozghatlian, The effect of cement composition and pH of environment on
641 sulfate resistance of Portland cements and blended cements, *Cement and Concrete Composites*. 19 (1997)
642 161–171. [https://doi.org/10.1016/S0958-9465\(97\)00011-5](https://doi.org/10.1016/S0958-9465(97)00011-5).
- 643 [14] Z. Shi, S. Ferreira, B. Lothenbach, M.R. Geiker, W. Kunther, J. Kaufmann, D. Herfort, J. Skibsted, Sulfate
644 resistance of calcined clay – Limestone – Portland cements, *Cement and Concrete Research*. 116 (2019)
645 238–251. <https://doi.org/10.1016/j.cemconres.2018.11.003>.
- 646 [15] A. Rossetti, T. Ikumi, I. Segura, E.F. Irassar, Sulfate performance of blended cements (limestone and illite
647 calcined clay) exposed to aggressive environment after casting, *Cement and Concrete Research*. 147 (2021)
648 106495. <https://doi.org/10.1016/j.cemconres.2021.106495>.
- 649 [16] M. Sahmaran, O. Kasap, K. Duru, I.O. Yaman, Effects of mix composition and water–cement ratio on the
650 sulfate resistance of blended cements, *Cement and Concrete Composites*. 29 (2007) 159–167.
651 <https://doi.org/10.1016/j.cemconcomp.2006.11.007>.
- 652 [17] S. Boudache, E. Rozière, A. Loukili, L. Izoret, Towards common specifications for low- and high-expansion
653 cement-based materials exposed to external sulphate attacks, *Construction and Building Materials*. 294
654 (2021) 123586. <https://doi.org/10.1016/j.conbuildmat.2021.123586>.
- 655 [18] Y.-J. Cha, W. Choi, O. Büyükköztürk, Deep Learning-Based Crack Damage Detection Using Convolutional
656 Neural Networks: Deep learning-based crack damage detection using CNNs, *Computer-Aided Civil and
657 Infrastructure Engineering*. 32 (2017) 361–378. <https://doi.org/10/f928ww>.
- 658 [19] S. Dorafshan, R.J. Thomas, M. Maguire, Comparison of deep convolutional neural networks and edge
659 detectors for image-based crack detection in concrete, *Construction and Building Materials*. 186 (2018)
660 1031–1045. <https://doi.org/10.1016/j.conbuildmat.2018.08.011>.
- 661 [20] Z. Liu, Y. Cao, Y. Wang, W. Wang, Computer vision-based concrete crack detection using U-net fully
662 convolutional networks, *Automation in Construction*. 104 (2019) 129–139.
663 <https://doi.org/10.1016/j.autcon.2019.04.005>.
- 664 [21] Y. Song, Z. Huang, C. Shen, H. Shi, D.A. Lange, Deep learning-based automated image segmentation for
665 concrete petrographic analysis, *Cement and Concrete Research*. 135 (2020) 106118.
666 <https://doi.org/10.1016/j.cemconres.2020.106118>.
- 667 [22] B. Hilloulin, I. Bekrine, E. Schmitt, A. Loukili, Modular Deep Learning Segmentation Algorithm for
668 Concrete Microscopic Images, *Construction and Building Materials*. 349 (2022).
669 <https://doi.org/10.1016/j.conbuildmat.2022.128736>.
- 670 [23] B. Hilloulin, I. Bekrine, E. Schmitt, A. Loukili, Open-source deep learning-based air-voids detection
671 algorithm for concrete microscopic images, *Journal of Microscopy*. (2022) jmi.13098.
672

- 673 <https://doi.org/10.1111/jmi.13098>.
- 674 [24] M. Liang, Y. Gan, Z. Chang, Z. Wan, E. Schlangen, B. Šavija, Microstructure-informed deep convolutional
675 neural network for predicting short-term creep modulus of cement paste, *Cement and Concrete Research*. 152
676 (2022) 106681. <https://doi.org/10.1016/j.cemconres.2021.106681>.
- 677 [25] B. Hilloulin, M. Lagrange, M. Duvillard, G. Garioud, ϵ -greedy automated indentation of cementitious
678 materials for phase mechanical properties determination, *Cement and Concrete Composites*. 129 (2022)
679 104465. <https://doi.org/10.1016/j.cemconcomp.2022.104465>.
- 680 [26] Y. Yu, W. Gao, A. Castel, A. Liu, X. Chen, M. Liu, Assessing external sulfate attack on thin-shell artificial
681 reef structures under uncertainty, *Ocean Engineering*. 207 (2020) 107397.
682 <https://doi.org/10.1016/j.oceaneng.2020.107397>.
- 683 [27] J.-S. Chou, C.-F. Tsai, A.-D. Pham, Y.-H. Lu, Machine learning in concrete strength simulations: Multi-
684 nation data analytics, *Construction and Building Materials*. 73 (2014) 771–780.
685 <https://doi.org/10.1016/j.conbuildmat.2014.09.054>.
- 686 [28] D.K. Bui, T. Nguyen, J.S. Chou, H. Nguyen-Xuan, T.D. Ngo, A modified firefly algorithm-artificial neural
687 network expert system for predicting compressive and tensile strength of high-performance concrete,
688 *Construction and Building Materials*. 180 (2018) 320–333.
689 <https://doi.org/10.1016/j.conbuildmat.2018.05.201>.
- 690 [29] M.J. Munir, S.M. Saleem Kazmi, Y.-F. Wu, X. Lin, M.R. Ahmad, Development of a novel compressive
691 strength design equation for natural and recycled aggregate concrete through advanced computational
692 modeling, *Journal of Building Engineering*. (2022) 104690. <https://doi.org/10.1016/j.job.2022.104690>.
- 693 [30] H.S. Ullah, R.A. Khushnood, J. Ahmad, F. Farooq, Predictive modelling of sustainable lightweight foamed
694 concrete using machine learning novel approach, *Journal of Building Engineering*. 56 (2022) 104746.
695 <https://doi.org/10.1016/j.job.2022.104746>.
- 696 [31] W.E. Elemam, A.H. Abdelraheem, M.G. Mahdy, A.M. Tahwia, Optimizing fresh properties and compressive
697 strength of self-consolidating concrete, *Construction and Building Materials*. 249 (2020) 118781.
698 <https://doi.org/10.1016/j.conbuildmat.2020.118781>.
- 699 [32] J. Karthikeyan, A. Upadhyay, N.M. Bhandari, Artificial Neural Network for Predicting Creep and Shrinkage
700 of High Performance Concrete, *ACT*. 6 (2008) 135–142. <https://doi.org/10.3151/jact.6.135>.
- 701 [33] P. Chen, W. Zheng, Y. Wang, W. Chang, Creep model of high-strength concrete containing supplementary
702 cementitious materials, *Construction and Building Materials*. 202 (2019) 494–506.
703 <https://doi.org/10.1016/j.conbuildmat.2019.01.005>.
- 704 [34] L. Bal, F. Buyle-Bodin, Artificial neural network for predicting drying shrinkage of concrete, *Construction
705 and Building Materials*. 38 (2013) 248–254. <https://doi.org/10.1016/j.conbuildmat.2012.08.043>.
- 706 [35] B. Hilloulin, V.Q. Tran, Using machine learning techniques for predicting autogenous shrinkage of concrete
707 incorporating superabsorbent polymers and supplementary cementitious materials, *Journal of Building
708 Engineering*. 49 (2022) 104086. <https://doi.org/10.1016/j.job.2022.104086>.
- 709 [36] B. Hilloulin, V.Q. Tran, Interpretable machine learning model for autogenous shrinkage prediction of low-
710 carbon cementitious materials, *Construction and Building Materials*. 396 (2023) 132343.
711 <https://doi.org/10.1016/j.conbuildmat.2023.132343>.
- 712 [37] R. Cai, T. Han, W. Liao, J. Huang, D. Li, A. Kumar, H. Ma, Prediction of surface chloride concentration of
713 marine concrete using ensemble machine learning, *Cement and Concrete Research*. 136 (2020) 106164.
714 <https://doi.org/10.1016/j.cemconres.2020.106164>.
- 715 [38] I. Nunez, M.L. Nehdi, Machine learning prediction of carbonation depth in recycled aggregate concrete
716 incorporating SCMs, *Construction and Building Materials*. 287 (2021) 123027.
717 <https://doi.org/10.1016/j.conbuildmat.2021.123027>.
- 718 [39] X. Wu, S. Zheng, Z. Feng, B. Chen, Y. Qin, W. Xu, Y. Liu, Prediction of the frost resistance of high-
719 performance concrete based on RF-REF: A hybrid prediction approach, *Construction and Building Materials*.
720 333 (2022) 127132. <https://doi.org/10.1016/j.conbuildmat.2022.127132>.
- 721 [40] S.M. Lundberg, S.-I. Lee, A Unified Approach to Interpreting Model Predictions, in: *Proceedings of the 31st
722 International Conference on Neural Information Processing Systems*, Curran Associates Inc., Red Hook, NY,
723 USA, 2017: pp. 4768–4777.
- 724 [41] A.K.S. T. H. Wee S.F. Wong, and A.K.M. Anisur Rahman, Sulfate Resistance of Concrete Containing

- 725 Mineral Admixtures, *ACI Materials Journal*. 97 (2000). <https://doi.org/10.14359/9286>.
- 726 [42] D.D. Higgins, Increased sulfate resistance of ggbs concrete in the presence of carbonate, *Cement and*
 727 *Concrete Composites*. 25 (2003) 913–919. [https://doi.org/10.1016/S0958-9465\(03\)00148-3](https://doi.org/10.1016/S0958-9465(03)00148-3).
- 728 [43] L. Courard, A. Darimont, M. Schouterden, F. Ferauche, X. Willem, R. Degeimbre, Durability of mortars
 729 modified with metakaolin, *Cement and Concrete Research*. 33 (2003) 1473–1479.
 730 [https://doi.org/10.1016/S0008-8846\(03\)00090-5](https://doi.org/10.1016/S0008-8846(03)00090-5).
- 731 [44] M. Zeljkovic, Metakaolin effects on concrete durability, University of Toronto, 2009.
- 732 [45] A. Bonakdar, B. Mobasher, Multi-parameter study of external sulfate attack in blended cement materials,
 733 *Construction and Building Materials*. 24 (2010) 61–70. <https://doi.org/10.1016/j.conbuildmat.2009.08.009>.
- 734 [46] H.N. Atahan, D. Dikme, Use of mineral admixtures for enhanced resistance against sulfate attack,
 735 *Construction and Building Materials*. 25 (2011) 3450–3457.
 736 <https://doi.org/10.1016/j.conbuildmat.2011.03.036>.
- 737 [47] W. Kunther, B. Lothenbach, K.L. Scrivener, On the relevance of volume increase for the length changes of
 738 mortar bars in sulfate solutions, *Cement and Concrete Research*. 46 (2013) 23–29.
 739 <https://doi.org/10.1016/j.cemconres.2013.01.002>.
- 740 [48] H. Siad, S. Kamali-Bernard, H.A. Mesbah, G. Escadeillas, M. Mouli, H. Khelafi, Characterization of the
 741 degradation of self-compacting concretes in sodium sulfate environment: Influence of different mineral
 742 admixtures, *Construction and Building Materials*. 47 (2013) 1188–1200.
 743 <https://doi.org/10.1016/j.conbuildmat.2013.05.086>.
- 744 [49] Ş. Yazıcı, H.Ş. Arel, D. Anuk, Influences of Metakaolin on the Durability and Mechanical Properties of
 745 Mortars, *Arab J Sci Eng*. 39 (2014) 8585–8592. <https://doi.org/10.1007/s13369-014-1413-z>.
- 746 [50] A.M. Hossack, M.D.A. Thomas, The effect of temperature on the rate of sulfate attack of Portland cement
 747 blended mortars in Na₂SO₄ solution, *Cement and Concrete Research*. 73 (2015) 136–142.
 748 <https://doi.org/10.1016/j.cemconres.2015.02.024>.
- 749 [51] F. Mittermayr, M. Rezvani, A. Baldermann, S. Hainer, P. Breitenbücher, J. Juhart, C.-A. Graubner, T.
 750 Proske, Sulfate resistance of cement-reduced eco-friendly concretes, *Cement and Concrete Composites*. 55
 751 (2015) 364–373. <https://doi.org/10.1016/j.cemconcomp.2014.09.020>.
- 752 [52] A. Trümer, H.-M. Ludwig, Sulphate and ASR Resistance of Concrete Made with Calcined Clay Blended
 753 Cements, in: K. Scrivener, A. Favier (Eds.), *Calcined Clays for Sustainable Concrete*, Springer Netherlands,
 754 Dordrecht, 2015: pp. 3–9. https://doi.org/10.1007/978-94-017-9939-3_1.
- 755 [53] H.Ş. Arel, B.S. Thomas, The effects of nano- and micro-particle additives on the durability and mechanical
 756 properties of mortars exposed to internal and external sulfate attacks, *Results in Physics*. 7 (2017) 843–851.
 757 <https://doi.org/10.1016/j.rinp.2017.02.009>.
- 758 [54] V. Bulatović, M. Melešev, M. Radeka, V. Radonjanin, I. Lukić, Evaluation of sulfate resistance of concrete
 759 with recycled and natural aggregates, *Construction and Building Materials*. 152 (2017) 614–631.
 760 <https://doi.org/10.1016/j.conbuildmat.2017.06.161>.
- 761 [55] A. Baldermann, M. Rezvani, T. Proske, C. Grengg, F. Steindl, M. Sakoparnig, C. Baldermann, I. Galan, F.
 762 Emmerich, F. Mittermayr, Effect of very high limestone content and quality on the sulfate resistance of
 763 blended cements, *Construction and Building Materials*. 188 (2018) 1065–1076.
 764 <https://doi.org/10.1016/j.conbuildmat.2018.08.169>.
- 765 [56] M. Sullivan, M. Chorzepa, H. Hamid, S. Durham, S. Kim, Sustainable Materials for Transportation
 766 Infrastructures: Comparison of Three Commercially-Available Metakaolin Products in Binary Cementitious
 767 Systems, *Infrastructures*. 3 (2018) 17. <https://doi.org/10.3390/infrastructures3030017>.
- 768 [57] Namik Kemal University, V. Akyuncu, M. Uysal, Istanbul University Cerrahpasa, H. Tanyildizi, Firat
 769 University, M. Sumer, Sakarya University, Modeling the weight and length changes of the concrete exposed
 770 to sulfate using artificial neural network, *Rdlc*. 17 (2019) 337–353. <https://doi.org/10.7764/RDLC.17.3.337>.
- 771 [58] F. Nosouhian, M. Fincan, N. Shanahan, Y.P. Stetsko, K.A. Riding, A. Zayed, Effects of slag characteristics
 772 on sulfate durability of Portland cement-slag blended systems, *Construction and Building Materials*. 229
 773 (2019) 116882. <https://doi.org/10.1016/j.conbuildmat.2019.116882>.
- 774 [59] X. Lv, Y. Dong, R. Wang, C. Lu, X. Wang, Resistance improvement of cement mortar containing silica fume
 775 to external sulfate attacks at normal temperature, *Construction and Building Materials*. 258 (2020) 119630.
 776 <https://doi.org/10.1016/j.conbuildmat.2020.119630>.

- 777 [60] A. Rossetti, T. Ikumi, I. Segura, E. Irassar, Sulfate Resistance of Blended Cements (Limestone Illite Calcined
778 Clay) Exposed Without Previous Curing, in: XV International Conference on Durability of Building
779 Materials and Components. EBook of Proceedings, CIMNE, 2020. <https://doi.org/10.23967/dbmc.2020.224>.
- 780 [61] Y. Yang, B. Zhan, J. Wang, Y. Zhang, W. Duan, Damage evolution of cement mortar with high volume slag
781 exposed to sulfate attack, *Construction and Building Materials*. 247 (2020) 118626.
782 <https://doi.org/10.1016/j.conbuildmat.2020.118626>.
- 783 [62] G. Cordoba, E.F. Irassar, Sulfate performance of calcined illitic shales, *Construction and Building Materials*.
784 291 (2021) 123215. <https://doi.org/10.1016/j.conbuildmat.2021.123215>.
- 785 [63] Q. Huang, X. Zhu, G. Xiong, M. Zhang, J. Deng, M. Zhao, L. Zhao, Will the magnesium sulfate attack of
786 cement mortars always be inhibited by incorporating nanosilica?, *Construction and Building Materials*. 305
787 (2021) 124695. <https://doi.org/10.1016/j.conbuildmat.2021.124695>.
- 788 [64] A. Rossetti, T. Ikumi, I. Segura, E.F. Irassar, Sulfate performance of blended cements (limestone and illite
789 calcined clay) exposed to aggressive environment after casting, *Cement and Concrete Research*. 147 (2021)
790 106495. <https://doi.org/10.1016/j.cemconres.2021.106495>.
- 791 [65] A. Schneider, G. Hommel, M. Blettner, Linear Regression Analysis, *Dtsch Arztebl Int*. 107 (2010) 776–782.
792 <https://doi.org/10.3238/arztebl.2010.0776>.
- 793 [66] Y. SONG, Y. LU, Decision tree methods: applications for classification and prediction, *Shanghai Arch*
794 *Psychiatry*. 27 (2015) 130–135. <https://doi.org/10.11919/j.issn.1002-0829.215044>.
- 795 [67] T. Chen, C. Guestrin, XGBoost: A Scalable Tree Boosting System, in: *Proceedings of the 22nd ACM*
796 *SIGKDD International Conference on Knowledge Discovery and Data Mining*, Association for Computing
797 Machinery, New York, NY, USA, 2016: pp. 785–794. <https://doi.org/10.1145/2939672.2939785>.
- 798 [68] G. Ke, Q. Meng, T. Finley, T. Wang, W. Chen, W. Ma, Q. Ye, T.-Y. Liu, LightGBM: A Highly Efficient
799 Gradient Boosting Decision Tree, in: *31st Conference on Neural Information Processing Systems (NIPS*
800 *2017)*, Long Beach, CA, USA, 2017.
- 801 [69] M. Liang, Z. Chang, Z. Wan, Y. Gan, E. Schlangen, B. Šavija, Interpretable Ensemble-Machine-Learning
802 models for predicting creep behavior of concrete, *Cement and Concrete Composites*. (2021) 104295.
803 <https://doi.org/10.1016/j.cemconcomp.2021.104295>.
- 804 [70] J. Bergstra, R. Bardenet, Y. Bengio, B. Kégl, Algorithms for hyper-parameter optimization, *Advances in*
805 *Neural Information Processing Systems*. (2011).
- 806 [71] M.T. Ribeiro, S. Singh, C. Guestrin, “Why Should I Trust You?”: Explaining the Predictions of Any
807 Classifier, in: *KDD*, San Francisco, CA, USA, 2016. <https://doi.org/10.48550/arXiv.1602.04938>.
- 808 [72] P.J.M. Monteiro, K.E. Kurtis, Time to failure for concrete exposed to severe sulfate attack, *Cement and*
809 *Concrete Research*. 33 (2003) 987–993. [https://doi.org/10.1016/S0008-8846\(02\)01097-9](https://doi.org/10.1016/S0008-8846(02)01097-9).
- 810 [73] H.N. Atahan, D. Dikme, Use of mineral admixtures for enhanced resistance against sulfate attack,
811 *Construction and Building Materials*. 25 (2011) 3450–3457.
812 <https://doi.org/10.1016/j.conbuildmat.2011.03.036>.
- 813 [74] P.J. Tikalsky, D. Roy, B. Scheetz, T. Krize, Redefining cement characteristics for sulfate-resistant Portland
814 cement, *Cement and Concrete Research*. 32 (2002) 1239–1246. [https://doi.org/10.1016/S0008-](https://doi.org/10.1016/S0008-8846(02)00767-6)
815 [8846\(02\)00767-6](https://doi.org/10.1016/S0008-8846(02)00767-6).
- 816 [75] E. Gruyaert, P. Van den Heede, M. Maes, N. De Belie, Investigation of the influence of blast-furnace slag on
817 the resistance of concrete against organic acid or sulphate attack by means of accelerated degradation tests,
818 *Cement and Concrete Research*. 42 (2012) 173–185. <https://doi.org/10.1016/j.cemconres.2011.09.009>.
- 819 [76] H. Binici, O. Aksoğan, Sulfate resistance of plain and blended cement, *Cement and Concrete Composites*. 28
820 (2006) 39–46. <https://doi.org/10.1016/j.cemconcomp.2005.08.002>.
- 821 [77] M.A. González, E.F. Irassar, Effect of limestone filler on the sulfate resistance of low C3A portland cement,
822 *Cement and Concrete Research*. 28 (1998) 1655–1667. [https://doi.org/10.1016/S0008-8846\(98\)00144-6](https://doi.org/10.1016/S0008-8846(98)00144-6).
- 823 [78] B. Persson, Sulphate resistance of self-compacting concrete, *Cement and Concrete Research*. 33 (2003)
824 1933–1938. [https://doi.org/10.1016/S0008-8846\(03\)00184-4](https://doi.org/10.1016/S0008-8846(03)00184-4).
- 825 [79] X. Lv, L. Yang, J. Li, F. Wang, Roles of fly ash, granulated blast-furnace slag, and silica fume in long-term
826 resistance to external sulfate attacks at atmospheric temperature, *Cement and Concrete Composites*. 133
827 (2022) 104696. <https://doi.org/10.1016/j.cemconcomp.2022.104696>.
- 828 [80] T. Aye, C.T. Oguchi, Resistance of plain and blended cement mortars exposed to severe sulfate attacks,

- 829 Construction and Building Materials. 25 (2011) 2988–2996.
830 <https://doi.org/10.1016/j.conbuildmat.2010.11.106>.
- 831 [81] T. Schmidt, B. Lothenbach, M. Romer, J. Neuenschwander, K. Scrivener, Physical and microstructural
832 aspects of sulfate attack on ordinary and limestone blended Portland cements, Cement and Concrete
833 Research. 39 (2009) 1111–1121. <https://doi.org/10.1016/j.cemconres.2009.08.005>.
- 834 [82] E.F. Irassar, V.L. Bonavetti, M. González, Microstructural study of sulfate attack on ordinary and limestone
835 Portland cements at ambient temperature, Cement and Concrete Research. 33 (2003) 31–41.
836 [https://doi.org/10.1016/S0008-8846\(02\)00914-6](https://doi.org/10.1016/S0008-8846(02)00914-6).
- 837 [83] X. Brunetaud, M.-R. Khelifa, M. Al-Mukhtar, Size effect of concrete samples on the kinetics of external
838 sulfate attack, Cement and Concrete Composites. 34 (2012) 370–376.
839 <https://doi.org/10.1016/j.cemconcomp.2011.08.014>.
- 840 [84] G. Massaad, E. Rozière, A. Loukili, L. Izoret, Do the geometry and aggregates size influence external sulfate
841 attack mechanism?, Construction and Building Materials. 157 (2017) 778–789.
842 <https://doi.org/10.1016/j.conbuildmat.2017.09.117>.
- 843 [85] A. Leemann, R. Loser, ACCELERATED SULFATE RESISTANCE TEST FOR CONCRETE -
844 CHEMICAL AND MICROSTRUCTURAL ASPECTS, (2012) 8.
- 845 [86] S. Boudache, A. Loukili, L. Izoret, E. Rozière, Investigating the role played by portlandite and C-A-S-H in
846 the degradation response of pozzolanic and slag cements to external sulphate attack, Journal of Building
847 Engineering. 67 (2023) 106053. <https://doi.org/10.1016/j.job.2023.106053>.
- 848 [87] M. Zeljkovic, Metakaolin effects on concrete durability, University of Toronto, 2009.

849

Highlights

- A database of concrete expansion under external sulfate attack is built
- Ensemble Machine learning models predict the expansion due to the external sulfate attack
- XGBoost is the most precise ensemble model for sulfate attack expansion prediction
- Inputs importance and relative influence can be assessed by SHAP
- Time to reach a given expansion can be inferred by the models

CRedit authorship contribution statement

Benoit Hilloulin: Conceptualization, Methodology, Investigation, Software, Formal analysis, Validation, Writing -original draft, Writing - review & editing, Supervision.

Abdelhamid Hafidi: Investigation, Software, Formal analysis, Writing -original draft.

Sonia Boudache: Validation, Writing -original draft, Writing - review & editing, Supervision.

Ahmed Loukili: Supervision, Project administration, Funding acquisition